ISTANBUL TECHNICAL UNIVERSITY ★ GRADUATE SCHOOL OF SCIENCE ENGINEERING AND TECHNOLOGY

FORWARD AND INVERSE SCATTERING PROBLEMS FOR THE OBJECTS LOCATED IN A CLOSED MEDIUM

M.Sc. THESIS

Gizem DİLMAÇ

Department of Electronics and Communications Engineering

Telecommunication Engineering Programme

JANUARY 2015

ISTANBUL TECHNICAL UNIVERSITY ★ GRADUATE SCHOOL OF SCIENCE ENGINEERING AND TECHNOLOGY

FORWARD AND INVERSE SCATTERING PROBLEMS FOR THE OBJECTS LOCATED IN A CLOSED MEDIUM

M.Sc. THESIS

Gizem DİLMAÇ
(504121318)

Department of Electronics and Communications Engineering

Telecommunication Engineering Programme

Thesis Advisor: Prof. Dr. Ali YAPAR

JANUARY 2015

İSTANBUL TEKNİK ÜNİVERSİTESİ ★ FEN BİLİMLERİ ENSTİTÜSÜ

KAPALI ORTAMLARA YERLEŞTİRİLEN OBJELERE İLİŞKİN DÜZ VE TERS SAÇILMA PROBLEMLERİ

YÜKSEK LİSANS TEZİ

Gizem DİLMAÇ
(504121318)

Elektronik ve Haberleşme Mühendisliği Anabilim Dalı

Telekomünikasyon Mühendisliği Programı

Tez Danışmanı: Prof. Dr. Ali YAPAR

OCAK 2015

Gizem DİLMAÇ, a **M.Sc.** student of ITU **Graduate School Of Science Engineering And Technology** 504121318, successfully defended the **thesis** entitled **"FORWARD AND INVERSE SCATTERING PROBLEMS FOR THE OBJECTS LOCATED IN A CLOSED MEDIUM"**, which she prepared after fulfilling the requirements specified in the associated legislations, before the jury whose signatures are below.

Thesis Advisor : **Prof. Dr. Ali YAPAR** ....
İstanbul Technical University

Jury Members : **Prof. Dr. Ali YAPAR** ....
İstanbul Technical University

Prof. Dr. Name SURNAME ....
Boğaziçi University

Prof. Dr. Name SURNAME ....
Gebze Institute of High Technology

Date of Submission : 22 December 2014
Date of Defense : 21 January 2015

To my parents and spouse,

FOREWORD

To begin with, I would like to express my sincerest gratitude to my advisor, Prof. Dr. Ali YAPAR whose help, advice and supervision were considerably precious. He gave me a great opportunity to improve my knowledge on inverse scattering.
I appreciated to TUBITAK for supporting me financially during graduate programme.
Finally, I am grateful to my spouse and parents for their support, patience and pray.

December 2014 Gizem DİLMAÇ
(Electronics and Communications Engineer)

TABLE OF CONTENTS

Page

FOREWORD .... **ix**
TABLE OF CONTENTS .... **xi**
ABBREVIATIONS .... **xiii**
LIST OF FIGURES .... **xv**
SUMMARY .... **xvii**
ÖZET .... **xix**
1. INTRODUCTION **1**
2. FORWARD PROBLEM **5**
2.1 Green's Function of Closed Medium 5
2.2 MoM Solution for The Scattered Field 7
2.3 Analytic Solution for A Special Case 11
3. INVERSE PROBLEM **15**
3.1 Born Approximation 15
3.1.1 Born approximation procedure 15
3.1.2 Born approximation for multi-source case 17
3.1.3 Born approximation - closed and unbounded medium 18
3.2 Newton Method 19
3.2.1 Newton procedure 19
3.2.2 Newton method for multi-source case 21
3.2.3 Newton method - closed vs. unbounded medium 22
4. NUMERICAL RESULTS **23**
4.1 Green's Function for Closed and Unbounded Mediums 23
4.2 A Verification of Scattered Field - Analytic vs. MoM 25
4.3 Born Approximation Results for Closed and Unbounded Mediums 26
4.4 Newton Method Results for Closed and Unbounded Mediums 34
5. CONCLUSIONS **41**
REFERENCES **43**
CURRICULUM VITAE **45**

ABBREVIATIONS

ε_0	: Free space permitivity
ε_b	: Relative dielectric permittivity of background
ε_{obj}	: Dielectric permittivity of object
ε_{robj}	: Relative dielectric permittivity of object
μ_0	: Free space permeability
σ_{obj}	: Conductivity of object
λ	: Wavelength
α	: Regularization (scaling) parameter
Ω	: Reconstruction domain
Γ	: Observation line
Δ_{pa}	: Distance between observers and PEC surrounding
Δ_{rp}	: Distance between reconstruction area and observers
J_n	: n^{th} order Bessel function of first kind
$H_n^{(1)}$	: n^{th} order Hankel function of first kind
$g(x,y)$	: Green's function of problem in Cartesian coordinates
g_c	: Green's function of closed medium
g_u	: Green's function of unbounded medium
k_b	: Wave number of lossless background medium
$u(y)$	: Total field
$u^i(y)$	: Incident field
$u^s(y)$	: Scattered field
$v(y)$	: Object function (contrast)

2D	: Two Dimensional
BA	: Born Approximation
BCs	: Boundary Conditions
CSI	: Contrast Source Injection
DE	: Data Equation
GF	: Green's Function
MoM	: Method of Moments
MR-CSI	: Multiplicative Regularized Contrast Source Injection
MWT	: Microwave Tomography
PEC	: Perfectly Electric Conducting
SVD	: Singular Value Decomposition
TM	: Transverse Magnetic

LIST OF FIGURES

Page

Figure 1.1 : A problem geometry. 2
Figure 2.1 : The discretized form of object. 9
Figure 2.2 : Visualization of DE's parameters. 10
Figure 2.3 : The scattering problem from dielectric circular cylinder and possible positions for an observer. 11
Figure 4.1 : A configuration for Green's Function comparison between closed and unbounded mediums [13]. 24
Figure 4.2 : Green's Function over a $10\text{-}cm^2$ cross section for (a) closed medium (b) in the absence of PEC cylinder. 24
Figure 4.3 : A sample configuration. 26
Figure 4.4 : Absolute of (a) Total field (b) Scattered field vs. observation points for an example visualized in Figure 4.3. 26
Figure 4.5 : First example with single line source for Born Approximation. 27
Figure 4.6 : The real parts of object function attained using single line source for (a) closed (b) free space medium. 28
Figure 4.7 : An example with multi line source for Born Approximation. 28
Figure 4.8 : The real parts of object function attained using multi line source for (a) closed (b) free space medium. 29
Figure 4.9 : A sample scenerio to observe effect of PEC radius. 29
Figure 4.10 : The real parts of object function acquired for Fig. 4.9 (a) PEC is removed (b) $\Delta\rho a=1.2\lambda$ (c) $\Delta\rho a=3.8\lambda$ (d) $\Delta\rho a=0.25\lambda$ (e) $\Delta\rho a=0.5\lambda$. 30
Figure 4.11 : A sample scenerio to explore the effect of reconstruction size (a) $L_\Omega =24\ cm$. (b) $L_\Omega=36\ cm$. 32
Figure 4.12 : The real parts of object function attained when reconstruction size is *24 cm* for (a) closed (b) free space medium. 32
Figure 4.13 : The real parts of object function attained when reconstruction size is *36 cm* for (a) closed (b) free space medium. 33
Figure 4.14 : An example involving two scatterers. 33
Figure 4.15 : The real parts of object function acquired for (a) closed (b) free space medium includes two scatterers ($\alpha=0.002$). 34
Figure 4.16 : The real parts of object function acquired for (a) closed (b) free space medium includes two scatterers ($\alpha=10^{-4}$). 34
Figure 4.17 : A high contrast object is inserted into a conducting enclosure. 35
Figure 4.18 : The real parts of object function obtained using BA for (a) closed (b) free space medium involves high contrast scatterer. 35
Figure 4.19 : The real parts of object function obtained using Newton method for (a) closed (b) free space medium involves high contrast scatterer. 36
Figure 4.20 : A square dielectric object exists in a conducting enclosure. 37
Figure 4.21 : The real parts of object function obtained for (a) closed (b) unbounded medium relative permittivity of *"3"*. 37

Figure 4.22 : A sample is to observe an effect of multi-scatterers using Newton method. 38
Figure 4.23 : The real parts of contrast obtained for (a) closed (b) unbounded medium having a relative permittivity of *"4"*. 38
Figure 4.24 : The real parts of contrast obtained for (a) closed $\|\delta\upsilon\| = 0.80$ (b) free space $\|\delta\upsilon\| = 0.80$ (c) free space $\|\delta\upsilon\| = 0.25$ medium. 39

FORWARD AND INVERSE SCATTERING PROBLEMS FOR THE OBJECTS LOCATED IN A CLOSED MEDIUM

SUMMARY

In this thesis, reconstruction of dielectric objects buried in a perfectly electric conducting enclosure is realized. Free space magnetic permeability is assumed for all cases. Our motivation is to observe the influence of reflected field from conducting boundary. It is predicted that reflections may form as image sources and hereby they result in better reconstruction. Primarily, synthetic data for scattered field is measured for arbitrary shaped objects. Then location, geometry and physical properties of scatterers are investigated for two cases: in an existing circular conducting boundary and in a free space. The approach used to solve this problem is based on a semi-numerical technique called method of moments (MoM). All implementations are coded in MATLAB environment.

MoM is a frequency domain solver that has been widely used since 1960s. It aims to discretize time-harmonic electromagnetic field integral equations and design a linear matrix system. Applying linear algebra, matrix equations can be solved at ease. Integral equation in MoM solution involves Green's function as its definition of Fredholm equation. Since Green's function is evaluated analytically, MoM is approved as a semi-numerical method.

Scattering problems are grouped into two categories such as forward and inverse scattering. Forward one is used to compute scattered field under the assumption of known source, scatterer and medium properties. Conversely, inverse one deals with acquiring the profile of objects when incident and scattered field data is known. Forward scattering problems are defined as well-posed problems; since their solution exists, is unique and stable. However, ill-posedness may arise for inverse scattering problems. Therefore, they need to be reformulated. Supplementary assumptions must be done to make the problem solvable. This operation is called regularization. A. N. Tikhonov proposed a regularization method that is recognized by his own name in 1963. During thesis, we benefit Tikhonov regularization to eliminate ill-posedness of problems.

Forward scattering problems concerning closed medium can be identified by an integral equation involving Green's function as it is mentioned. Therefore, we begin with finding Green's function of closed medium. Then, scattered field is calculated numerically. Integral equation is discretized and total field is computed for each cell. The decrease in cell size serves better object modeling, so cell side is chosen at most $\lambda/16$. Accuracy of MoM process is very important for us and verification is necessary. For this purpose, analytic solution for closed medium is also performed. By the way, Green's function is employed as a 2D transverse magnetic (TM) polarized line source. When a single source is injected into simulation area, some deficiencies are encountered in imaging. Therefore, multi-source illumination is

preferred in most cases. Besides, plenty of observers are located around the scatterer in a certain distance.

Next, inversion algorithm is applied to achieve shape reconstruction. By doing so, Born Approximation and Newton methods are utilized. Born Approximation requires some restrictions to be satisfied. It provides improvements in outcomes if operating frequency and/or contrast are low. To explore object function, Born method enables us to use incident field in integral (data) equation instead of total one. In other words, scattered field is ignored. Then, discretization is performed for integral equation. However, ill-posedness is shown up while applying linear algebra. Hence, Tikhonov regularization is implemented. On the other hand, Newton method does not need any provision, so it is more advanced. It is an iterative method presented to find object function. It starts with guessing an initial value for sought object function. In every step, a new guess object function is proposed to reach or get close to real value of it. We selected a condition for error tolerance to halt the process when object function is close enough to real value.

After reconstruction for closed medium is fulfilled, conducting surrounding is removed. Forward and inverse problems are solved for unbounded medium using appropriate Green's function. The background medium can be a free space or dielectrically filled.

Several tests are practiced to observe the impact of conducting boundary on reconstruction and localization of object in closed mediums. The selection of radius of conducting enclosure is very important. The most favorable distance between observers and conducting enclosure *"λ/4"* is also affirmed. In addition, size of reconstruction area is examined. Born method offers us quality imaging for particular cases. The increase in contrast deteriorates the results. Therefore, Newton method is also applied to same settings. The drawback of Newton is to find a convenient initial value for contrast. If it is not picked properly in the beginning, simulation duration lasts longer or forever.

In conclusion, forward problem is verified by means of analytic solution. Born and Newton methods are successfully performed for inversion. The reconstruction and localization is succeeded. Multi-source effect is analyzed and its performance is highlighted. Unfortunately closed medium solutions do not provide great enhancement in imaging as supposed. For most cases, shape reconstruction is not corrupted at least. There has to be some advantages of closed mediums, because they preserve the simulation area.

PEC İLE ÇEVRELENMİŞ KAPALI ORTAMLARA YERLEŞTİRİLEN OBJELERE İLİŞKİN DÜZ VE TERS SAÇILMA PROBLEMLERİ

ÖZET

Bu tez çalışmasında, mükemmel iletken bir yüzey ile kapatılan ortamlara gömülü dielektrik cisimlerin görüntülenmesi gerçekleştirilmiştir. Tüm örneklerde boş uzay manyetik geçirgenliği kullanılmıştır. Boş uzayın iletken bir yüzey ile çevrelenerek incelenmesindeki amaç, yüzeylerden yansıyacak alanların etkisini gözlemleyebilmektir. Oluşan yansımaların görüntü kaynakları gibi davranarak daha iyi sonuçlar ortaya çıkaracağı öngörülmüştür. Öncelikle keyfi cisimler için saçılan alan hesabı güçlü bir nümerik yöntem olan Momentler Metodu yardımı ile yapılmıştır. Daha sonra saçıcıların konumu, geometrisi ve fiziksel özellikleri, iletken çevrelemenin olduğu ve olmadığı iki farklı ortam için ayrı ayrı bulunmuştur. Tüm uygulamalar MATLAB ortamında gerçekleştirilmiştir.

Momentler Metodu 1960'lardan beri yaygın olarak kullanılan bir frekans domeni çözücüdür. MoM teorisi, zamanda harmonik elektromanyetik alan integral denklemlerini ayrıklaştırarak lineer bir matris sistemi tasarlamayı hedeflemektedir. Lineer cebir teknikleri uygulanarak, problem matris denklemleri için kolaylıkla çözülebilmektedir. MoM çözümündeki integral denklemi Fredholm denkleminin tanımı gereği Green fonksiyonu içermektedir. Green fonksiyonu analitik olarak hesaplandığı için MoM yarı nümerik bir metot olarak kabul edilmektedir.

Saçılma problemleri düz ve ters saçılma problemleri olmak üzere iki kategoriye ayrılmıştır. Düz saçılma bilinen gelen alan (kaynak), saçıcı ve ortam parametreleri kabulü altında saçılan alanları hesaplamaktadır. Diğer taraftan, ters saçılma gelen ve saçılan alanların bilindiği durumlarda cisim profillerinin elde edilmesiyle ilgilenmektedir. Düz saçılma problemleri iyi tanımlanmış problemlerdir; bu yüzden çözümleri vardır, tektir ve kararlıdır. Ancak ters saçılma problemleri için kötü koşulluluk (ill-conditioned) olarak bilinen başlangıç verisindeki küçük hataların sonuçta çok büyük hatalara sebep olması durumu ortaya çıkabilmektedir. Çözüm matris sisteminde gerçekleştirildiği için, koşul sayısının çok büyük olduğu hallerde matrisler kötü koşullu olabilmektedir. Bu yüzden, ters problemlerin yeniden formüle edilmesi gerekmektedir. Problemi çözülebilir hale getirebilmek için ek varsayımlar yapılmalıdır. Bu işleme regülarizasyon denilmektedir. 1963 yılında A. N. Tikhonov kendi soyadıyla anılan bir regülarizasyon yöntemi önermiştir. Bu tezdeki örneklerde ortaya çıkmış olan tüm kötü koşulluluk durumları Tikhonov regülarizasyonundan yararlanılarak yok edilmiştir.

Bu çalışmada öncelikle kapalı ortamlara gömülü cisimlere ilişkin ters saçılma problemi, ilgili Green fonksiyonu yardımıyla bir integral denklem sistemi şeklinde ifade edilmiştir. İlgili Green fonksiyonu silindirik harmonikler cinsinden bir seri ile analitik olarak bulunmuştur. Probleminin formülasyonundaki integral denklem düz problemi de ifade ettiğinden, öncelikle düz problem kanonik bir yapı için Momentler Metodu ile çözülmüştür ve saçılan alanlar elde edilmiştir. Bahsedildiği gibi

Momentler Metodu uygulanırken integral denklemi ayrıklaştırılarak her bir hücre için toplam alan hesabı yapılır. Hücre boyutlarını olabildiğince küçük seçmek cisimlerin daha iyi modellenmesini sağlayacaktır. Bu çalışmadaki örneklerde kullanılan objeler kenar uzunlukları en çok *λ/16* olan karesel hücrelere ayrılmıştır. Cismin olabildiğince küçük parçalara ayrılması elbette önemlidir ama matrislerdeki aşırı büyümeler hesaplama yükünü arttırmaktadır ve MATLAB ortamında işlem yapmak mümkün olamamaktadır. Bu yüzden, hücre boyutları genelde *λ/10* ile *λ/20* arasında seçilmektedir. MoM yönteminin formülasyonunun ve ölçülen saçılan alan verisinin doğruluğu çok önemlidir. Nümerik yöntemin doğruluğunu teyit etmek için dairesel silindirik bir objeye ilişkin analitik çözüm gerçekleştirilmiştir. Green fonksiyonu iki boyutlu enine manyetik polarize çizgisel bir kaynak olarak kullanılmıştır. Görülmüştür ki simülasyon alanına tek bir çizgisel kaynak enjekte edildiği durumlarda cisim görüntülenmesi yapılırken bazı durumlarda iyi sonuçlar ortaya çıkmamaktadır. Bu sebeple, çoğu örnekte cisimler birden çok kaynak yardımıyla uyarılmıştır. Dahası, birden çok gözlem noktası saçıcının etrafına eşit aralıklarla yerleştirilmiştir.

Düz problem çözümü yapılıp saçılan alanlar ölçüldükten sonra kapalı ortamlara gömülü cisimlerin konumları ve fiziksel özelliklerinin belirlenmesi için probleme tersleme algoritmaları uygulanmıştır. Ters saçılma problemi ilk olarak ancak özel bazı kısıtlama ve koşullarda geçerli, fakat oldukça basit bir yöntem olan Born Yaklaşımı ile daha sonra da daha genel bir metot olan Newton yöntemi ile çözülmüştür. Born Yaklaşımı, çalışma frekansı ve aranan cisim fonksiyonunun düşük olduğu durumlarda iyi sonuçlar vermektedir. Born metodu cisim fonksiyonunu bulmak için, problemin integral denklemindeki toplam alanlar yerine sadece gelen alan verisi yazılmasına olanak sağlamaktadır. Diğer bir deyişle, saçılan alanların ihmal edilebilecek kadar küçük olduğu varsayılmaktadır. Daha sonra düz problem çözümünde olduğu gibi integral denklem ayrıklaştırılır ve matris sistemine geçilir. Ama önceden de bahsedildiği gibi lineer cebir teknikleri uygulanırken bazı kötü koşullu matrislerle karşılaşılmaktadır. Bu sebeple Tikhonov regülarizasyonu uygulanmıştır. Diğer yandan, Newton metodu herhangi bir koşul gerektirmez, bu yüzden daha gelişmiş bir metot olarak kabul edilir. Newton yöntemi, cisim fonksiyonun bulunması için sunulmuş iteratif bir yaklaşımdır. Aranan cisim fonksiyonu için bir başlangıç değerinin belirlenir. Metot, gerekli adımları tekrarlayarak gerçek değere yaklaşmayı hedeflemektedir. Her döngü de cisim fonksiyonu güncellenmektedir ve belirli bir hata olasılığına göre gerçek değere yeteri kadar yaklaşıldığında döngü durdurulmaktadır.

Ters saçılma probleminin çözümü kapalı ortamlar için verildikten sonra mükemmel iletken yüzey kaldırılır. Düz ve ters problem çözümü boş uzay için uygun Green fonksiyonu yardımıyla gerçekleştirilir. Cisimlerin yerleştirildiği ortam boş uzay olabileceği gibi dilektrik bir malzeme ile de doldurulmuş olabilir.

Mükemmel iletkenlerle kapatılan ortamların, cisimlerin konum ve fiziksel özelliklerinin belirlenmesindeki etkileri birçok örnek yardımıyla test edilmiştir. Burada, iletken yüzeyin yarıçapının seçimi çok önemlidir. Gözlem noktaları ve iletken tabaka arasındaki en uygun uzaklığın *λ/4* olduğu kabul edilir ve bu gerçek örneklerle desteklenmiştir. Tersleme algoritmasının uygulanması için belirlenen yüzey alanın büyüklüğü de ayrıca incelenmiştir. Born Yaklaşımı belirli durumlar için iyi sonuç vermektedir. Cisim fonksiyonundaki artış ile birlikte sonuçlar kötü yönde etkilenmekte ve cismin görüntülenmesi mümkün olmamaktadır. Bu yüzden, aynı konfigürasyon ve ortam parametreleri için Newton metodu uygulanmıştır. Newton yönteminin zayıf yönü ise cisim fonksiyonu için uygun bir başlangıç koşulu seçilmediği takdirde çözüme ulaşmanın çok uzun süre alabilecek olmasıdır. Bunlar dışında, ortamda birden çok saçıcı var iken Born ve Newton metotlarıyla cisim görüntülenmesi gerçekleştirilmiştir.

Kısaca toparlamak gerekirse, ilk olarak düz problem çözümünün doğruluğu analitik yöntemler yardımıyla kontrol edilmiştir. Ters problem çözümünde Born Yaklaşımı ve Newton yöntemleri başarılı bir şekilde uygulanmıştır. Mükemmel iletken ile kapatılan ortamlara yerleştirilen cisimlerin konum, geometri ve fiziksel özellikleri elde edilmiştir. Maalesef kapalı ortamlar varsayıldığı gibi saçıcıların belirlenmesinde büyük iyileştirmeler sağlayamamıştır. En azından çoğu örnek için büyük zararlar da vermemektedir. Dielektrik veya iletken sınırlar simülasyon alanını etkileşimlerden korumaktadır, bundan dolayı bazı avantajları olmalıdır.

1. INTRODUCTION

Inverse scattering problems deal with retrieval of object profile exploiting scattered field. Plenty of numerical methods are developed to achieve reconstruction of scatterers. Most popular techniques are explained in [1-4]. The advance in technology allows researchers apply inversion algorithms to variety of fields at ease. Some of the practical application areas are medical imaging, geophysics, space research, remote sensing, and image processing.

The easiest case for inverse scattering problems is related to unbounded medium, which means only scatterers exist in simulation space. Any kind of incident field excites the objects and scattered field is measured. Using scattered field, the geometry, physical properties and location can be revealed. However, in practice there can be undesired reflectors such as walls, surfaces and other materials. As an example, it can be needed to investigate objects behind the walls (through wall imaging - TWI) or under the ground [5,6].

Most inverse problems are defined as ill-posed unlike forward ones. A French mathematician J. Hadamard propounded the definition of well-posedness [7]. According to him, if a problem is solvable, its solution is unique and stable; then this problem is approved as well-posed. Forward scattering problems are in this category. On the other hand, inverse problems represented by first kind of Fredholm equation are ill-posed. There are several methods to overcome ill-posedness such as singular value decomposition [8] and regularization [9]. Thanks to regularization, additional terms are inserted to solution and problem is tried to approach a well-posed one. Here, one of the most widely used methods, Tikhonov regularization [10], is employed.

The impact of existence of enclosures has become a hot topic in recent years because of its success of modeling biomedical imaging particularly. In this thesis, we proposed an electrically conducting surrounded configuration to enhance our imaging. Reconstruction in a closed medium is examined before [11,12], but it is mostly preferred to use dielectric surfaces for enclosures. There are few researches on conducting surfaces [13,14]. The idea of enclosures is largely utilized for diagnosis of abnormalities in tissues (e.g. tumors) that relates to microwave tomography (MWT) [15]. Therefore, we constitutively concentrate on targets embedded inside a PEC shape. From one point, reflected field from boundaries acts as multi-sources, so imaging can be improved. In addition, PEC boundary prevents some interactions can be experienced in unbounded mediums. Briefly, we aim to research into usage of surroundings provides us enhancement in reconstruction or not.

Our concern related to identification of 2D arbitrary dielectric cylinders $(\varepsilon_{obj}, \sigma_{obj}, \mu_0)$ enclosed by a circular PEC surface is visualized in Figure 1.1. It is assumed that infinite long cylinders are taken into account. Thus, 3D problem is reduced to 2D by neglecting changes on one dimension. The circular PEC cylinder radius of *"a"* can be filled by a free space (ε_0) or lossless dielectric background (ε_b). However, free space magnetic permeability *"μ_0"* is used in both targets and background for all cases. Targets are excited by a 2D TM polarized single line source at first. However, it is known that multi-sources provide better reconstruction. Thus, array of sources are equally placed on circle with radius *"c"*. In addition, plenty of observers are laid on a circle.

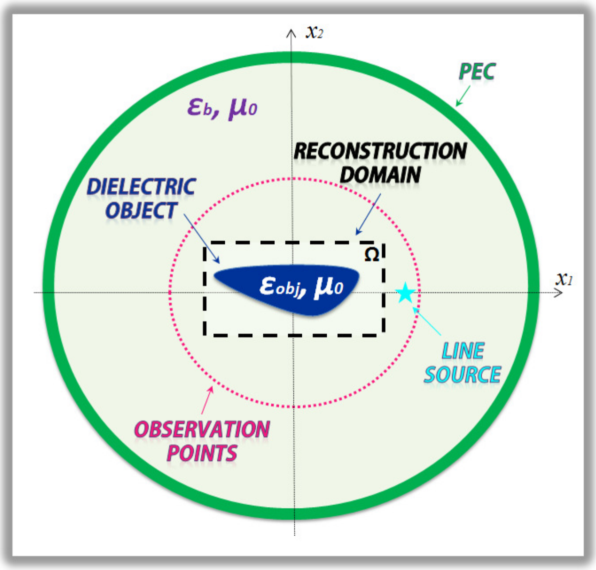

Figure 1.1 : A problem geometry.

Solution to exploration of few certain shapes can be found via analytical and numerical ways. A dielectric circle is one of them. However, arbitrary shaped objects can only be reconstructed using numerical methods so we benefit from methods of moment. Thus, the problem is defined as an integral equation including Green's function. Section 2 starts with evaluation of Green's function of closed medium and goes on forward problem solution using MoM. To measure scattered field, MoM procedure requires discretization of integral equation and transformation to matrix system. All scatterers are divided into small segments where electric field along a cell remains constant. The smaller cell size enables us to model object in a better way, so it is commonly selected around $\lambda_{min}/10 \sim \lambda_{min}/20$. Total field for each cell using object equation is computed. After, scattered field in observers is measured through discretized form of data equation (DE). MoM process for arbitrary objects is put forward by Richmond and presented in details [16]. Furthermore, analytic solution allows us to verify our numeric result is correct or not. Section 2 ends with analytical solution of scattered field for a special case.

Moreover, two of the inversion algorithms that are Born Approximation and Newton methods are applied to reconstruct scatterers. Born method has some conditions to be hold if improved imaging is desired. The operating frequency and/or contrast of sought object are low, and then this method works well. To perform an inversion, a suitable reconstruction domain (Ω) that probably includes scatterers must be designated. The scattered field is described as a DE involving the points in reconstruction and observation. This integral is also discretized like forward problem solution. Born method provides us to use incident field in DE instead of total one neglecting scattered field. Since our problem is inverse, ill-conditioning is aroused while applying linear algebra. Hence, Tikhonov regularization technique is utilized to eliminate ill-posedness. Although Newton gains an advantage over Born Approximation, it has also a handicap. Newton method is required to estimate initial value for contrast. Then, it is tried to approach real value iteratively. In each iteration, a new contrast is offered, so the choice of estimated contrast is very vital. In addition, we specify an error tolerance to stop the iteration when the estimated contrast is close enough to real value. Besides, ill-posedness is encountered again and Tikhonov regularization is applied for Newton case. Section 3 is allocated to inverse scattering techniques for both Born Approximation and Newton. In addition, their multi-sources formulations are given.

In section 4, various tests are done to find out the influence of PEC surface on imaging in closed mediums. The object reconstruction is also carried out in unbounded mediums for comparisons. Forward and inverse problems are solved using a proper Green's function. The background may be free space or dielectrically filled. First part of section 4, Green's function related to PEC enclosure is studied. Ref. [13] gives an example to observe the Green's function of many observers placed on a rectangular shape. Here, a similar modeling is implemented and results are compared. Secondly, using an analytic method we make sure our outcomes are acceptable. Last two subheadings are interested in examples of Born and Newton inversion methods. A PEC enclosed system in [13] is established and reconstruction is done. Ref [13] is very beneficial for us to check ourselves.

The values of design parameters in Section 4.3 and 4.4 are selected intentionally for most cases. To enhance reconstruction one needs to pay attention choices of measurement system parameters. For this purpose, Crocco and Litman published a paper [17] refers the design parameters of closed and unbounded mediums. According to them, the most appropriate distance between radius of observers and PEC boundary is *"$\lambda/4$"*. Moreover, the size of reconstruction area should be far away from observers more than a half wavelength. As it is mentioned before, Born method provides good inversion for particular cases such as in low operating frequency. Ref. [13] gives some examples on MWT, so they are compared using Newton procedure.

In section 5, thesis is concluded by means of extended analysis of all collected outcomes.

2. FORWARD PROBLEM

Forward problem concerns acquiring scattered field by use of incident wave and known properties of scatterers. Even if this thesis is intended to solve inverse problems related to closed medium, scattered field computations are inevitable. For this reason, we start with finding Green's function (GF) of closed medium. GF for free space has already explained in [18], so this section will clarify formulations relevant to PEC enclosures. Moment solution for scattered field in free space is discussed in [16] in-depth. Here, we will carry out similar steps regarding reflected fields from PEC boundary. Lastly, analytic solution for closed medium will be submitted.

2.1 Green's Function of Closed Medium

Green's function satisfies inhomogeneous Helmholtz equation when the right side of equation is source function. 2D line source can be expressed using Dirac's function.

$$\begin{aligned} \nabla^2 g(x;y) + k^2 g(x;y) &= -\delta(x - y) \\ &= -\delta(x_1 - y_1)\delta(x_2 - y_2) \end{aligned} \qquad \textbf{(2.1)}$$

where *"$x(x_1, x_2)$"* is observer, *"$y(y_1, y_2)$"* is source in 2D Cartesian coordinates.

GF can be described as infinite series summation in terms of cylindrical harmonics. When observers are placed between sources and PEC boundary, both standing and outgoing waves exist. If radius of observation points is smaller than sources', only standing waves occur. These two facts and Fourier series expansion allow us to identify Green's function. It is written as in cylindrical coordinates:

$$g(\rho,\phi;\rho',\phi') = \frac{1}{2\pi}\sum_{n=-\infty}^{\infty} \hat{g}(\rho,n;\rho',\phi')e^{in\phi} \qquad \textbf{(2.2)}$$

$$\hat{g}(\rho,n;\rho',\phi')=\begin{cases}A_nH_n^{(1)}(k\rho)+B_nJ_n(k\rho) & , \ \rho'\le\rho\le a \\ C_nJ_n(k\rho) & , \ 0\le\rho\le\rho'\end{cases} \quad \textbf{(2.3)}$$

where (ρ,n) shows observation point, (ρ',ϕ') relates to source in cylindrical coordinates and *"a"* is radius of PEC surrounding. J_n and $H_n^{(1)}$ are the Bessel and Hankel functions of first kind respectively. As it is seen from Equation **(2.3)**, standing waves are represented using Bessel function and outgoing ones are declared through Hankel function. Let us insert Equation **(2.3)** into **(2.2)**:

$$g(\rho,\phi;\rho',\phi')=\begin{cases}\frac{1}{2\pi}\sum_{n=-\infty}^{\infty}\left[A_nH_n^{(1)}(k\rho)+B_nJ_n(k\rho)\right]e^{in\phi} & , \ \rho'\le\rho\le a \\ \frac{1}{2\pi}\sum_{n=-\infty}^{\infty}C_nJ_n(k\rho)e^{in\phi} & , \ 0\le\rho\le\rho'\end{cases} \quad \textbf{(2.4)}$$

There are three unknown coefficients in Eq. **(2.4)**. Therefore, matching and boundary conditions are written down to find coefficients. Equations **(2.5a)** and **(2.5b)** are matching conditions for source point (ρ',ϕ'). The boundary condition in surface of PEC enclosure is given in Eq. **(2.5c)**.

$$\hat{g}(\rho=\rho'+0)-\hat{g}(\rho=\rho'-0)=0 \quad \textbf{(2.5a)}$$

$$\frac{\partial\hat{g}}{\partial\rho}(\rho=\rho'+0)-\frac{\partial\hat{g}}{\partial\rho}(\rho=\rho'-0)=\left.\frac{-1}{\rho}e^{-in\phi'}\right|_{\rho=\rho'}=\frac{-1}{\rho'}e^{-in\phi'} \quad \textbf{(2.5b)}$$

$$\hat{g}(\rho=a)=0 \quad \textbf{(2.5c)}$$

Equations from **(2.5a)** to **(2.5c)** are realized using definition of $\hat{g}$ given in Eq. **(2.3)**. Three equations for three unknowns are solved for A_n, B_n and C_n.

$$\begin{aligned}A_n&=\frac{i\pi}{2}J_n(k\rho')e^{-in\phi'}\\ B_n&=\frac{-i\pi}{2}\frac{H_n^{(1)}(ka)}{J_n(ka)}J_n(k\rho')e^{-in\phi'}\\ C_n&=\frac{i\pi}{2}\left[H_n^{(1)}(k\rho')-\frac{H_n^{(1)}(ka)}{J_n(ka)}J_n(k\rho')\right]e^{-in\phi'}\end{aligned} \quad \textbf{(2.6)}$$

After finding coefficients, Eq. **(2.4)** is revisited and incident and reflected parts are separated.

$$g(\rho,\phi;\rho',\phi')=\begin{cases} g_{inc1}+g_{ref} \ , & \rho'\leq\rho\leq a \\ g_{inc2}+g_{ref} \ , & 0\leq\rho\leq\rho' \end{cases} \tag{2.7}$$

where

$$\begin{aligned} g_{inc1} &= \frac{i}{4}\sum_{n=-\infty}^{\infty} J_n(k\rho')H_n^{(1)}(k\rho)e^{in(\phi-\phi')} \\ g_{inc2} &= \frac{i}{4}\sum_{n=-\infty}^{\infty} H_n^{(1)}(k\rho')J_n(k\rho)e^{in(\phi-\phi')} \\ g_{ref} &= -\frac{i}{4}\sum_{n=-\infty}^{\infty} \frac{H_n^{(1)}(ka)}{J_n(ka)}J_n(k\rho')J_n(k\rho)e^{in(\phi-\phi')} \end{aligned} \tag{2.8}$$

Equation **(2.8)** is also known fact from Addition Theorem [19].

$$\begin{aligned} &\frac{i}{4}H_0^{(1)}(k|\rho - \rho'|)=\frac{i}{4}\sum_{n=-\infty}^{\infty} J_n(k\rho_>)H_n^{(1)}(k\rho_<)e^{in(\phi-\phi')} \\ &where \quad \rho_> = max(\rho,\rho') \ , \ \rho_< = min(\rho,\rho') \end{aligned} \tag{2.9}$$

Eq. **(2.6)** can be represented in a compact form:

$$\begin{aligned} g(\rho,\phi;\rho',\phi') &= \frac{i}{4}H_0^{(1)}(k|\rho - \rho'|) \\ &\quad -\frac{i}{4}\sum_{n=-\infty}^{\infty} \frac{H_n^{(1)}(ka)}{J_n(ka)}J_n(k\rho')J_n(k\rho)e^{in(\phi-\phi')} \ , \ 0\leq\rho\leq a \end{aligned} \tag{2.10}$$

2.2 MoM Solution for The Scattered Field

When incident wave hits an object, it causes induced current. This current creates scattered field that can be pointed out in Cartesian coordinate as following:

$$u^s(x)=k_b^2\int_D g(x,y)v(y)u(y)dy \qquad x\in\Gamma \tag{2.11}$$

Here, *"$x(x_1,x_2)$"* is observation point and source is denoted by *"$y(y_1,y_2)$"*. *"$g(x,y)$"* is GF of problem. *"k_b"* is wave number of lossless background medium and *"$v(y)$"* is object function (contrast) and their definitions are given in Equation **(2.12**). Total field is demonstrated by *"u(y)"*.

$$v(y) = \frac{k_{obj}^2(y)}{k_b^2(y)} - 1 \quad ; \quad y \in D \tag{2.12}$$

$$where \;\; k_{obj}^2(y) = \omega^2 \varepsilon_{obj} \mu_0 + i\omega\sigma(y)\mu_0 \;\; and \;\; k_b^2(y) = \omega^2 \varepsilon_b \mu_0$$

Total field is sum of incident and reflected field. Thanks to this property, the unknown total field in scatterer is separated from known incident field **(2.13)**. *"* $\varepsilon_{r_{obj}}$ *"* is relative permittivity of object. It is used in object function formula obtained via Equation **(2.12)**.

$$u(x) - k_b^2 \int_D g(x,y)(\varepsilon_{r_{obj}} - 1)u(y)dy = u^i(x) \quad x \in D \tag{2.13}$$

In previous section, GF of closed medium is found in cylindrical coordinates. Thus, Equation **(2.13)** is also converted to cylindrical one.

$$u(\rho) - k_b^2 \int_D g(\rho,\rho')(\varepsilon_{r_{obj}} - 1)u(\rho')\rho' d\rho' d\phi' = u^i(\rho) \quad \rho \in D \tag{2.14}$$

Even if the object equation is transformed, it still is not possible to calculate total field. In order to succeed in our objective, cross section area of arbitrary target is divided into small rectangular segments where field component is constant. Then, total field in integration can be extracted and integration is carried out at ease. The discretized case is given below:

$$u_m(\rho) - k_b^2 \sum_{n=1}^{N} \int_{D_n} g(\rho,\rho')(\varepsilon_{n_{obj}} - 1)u_n(\rho')\rho' d\rho' d\phi' = u_m^i(\rho) \tag{2.15}$$

Now, the equation can be demonstrated in terms of system of linear equations. The total cell number is selected as *"N"*.

$$\sum_{n=1}^{N} C_{mn} u_n = u_m^i \quad where \;\; m = 1,2,...,N \tag{2.16}$$

The entities of *"C"* matrix are found by integration of GF (see Equation **(2.15)**). GF of closed medium is composed of two parts. The first one is free space term and another is aroused from reflections from PEC boundaries. Integration of free space part is given in Ref [16] in details. This part is directly adopted from there. For reflected one, there is no singularity in integration. Therefore, it is enough to compute the "g_{ref}" in Eq. **(2.8)** and multiply by cell size. The entities of "C" matrix are specified in Eq. **(2.17)**. "ρ'" and "ϕ'" are radius of source from origin and angle of it, whereas "ρ" and "ϕ" are observation point's properties (see Figure 2.1). While evaluating integration, rectangular cells must be converted to circular one [16], so radius of circular cells "a_m" is needed to find. "Δx_1" and "Δx_2" are lengths of cell's side.

$$C_{mn} = \begin{cases} 1+(\varepsilon_{m_{obj}}-1)(-i/2)[\pi k_b a_m H_1^{(1)}(k_b a_m)+2i] & ,n=m \\ +\dfrac{ik^2}{4}(\varepsilon_{n_{obj}}-1)\Delta x_1\Delta x_2 \displaystyle\sum_{nn=-\infty}^{\infty}\dfrac{H_{nn}^{(1)}(k_b a)}{J_{nn}(k_b a)}J_{nn}(k_b\rho')J_{nn}(k_b\rho)e^{inn(\phi-\phi')} & \\ (-i\pi k_b a_m/2)(\varepsilon_n-1)J_1(k_b a_n)H_0^{(1)}(k_b\rho_{mn}) & ,n\neq m \\ +\dfrac{ik^2}{4}(\varepsilon_{n_{obj}}-1)\Delta x_1\Delta x_2 \displaystyle\sum_{nn=-\infty}^{\infty}\dfrac{H_{nn}^{(1)}(k_b a)}{J_{nn}(k_b a)}J_{nn}(k_b\rho')J_{nn}(k_b\rho)e^{inn(\phi-\phi')} & \end{cases} \quad \textbf{(2.17)}$$

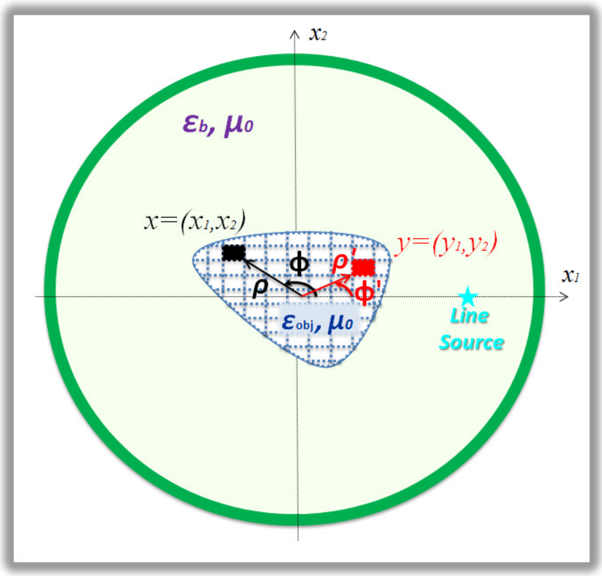

Figure 2.1 : The discretized form of object.

The formulations of source and object parameters are written in following:

$$\rho' = \sqrt{y_1^2 + y_2^2} \quad \phi' = atan2(y_2/y_1) \quad \textbf{(2.18)}$$
$$\rho = \sqrt{x_1^2 + x_2^2} \quad \phi = atan2(x_2/x_1)$$

Total field for each cell is calculated by:

$$u = C^{-1}u^{i} \tag{2.19}$$

Next, scattered field is found through DE **(2.20)**. Spatial parameters in DE are pictured in Figure 2.2. *"x"* is a vector sized *"Rx1"* and its elements are on measurement line *"Γ"*. The size of *"y"* is *"Nx1"* and they denote center points of each cell in object. *"z"* is a vector sized by *"Qx1"* and related to 2D line sources.

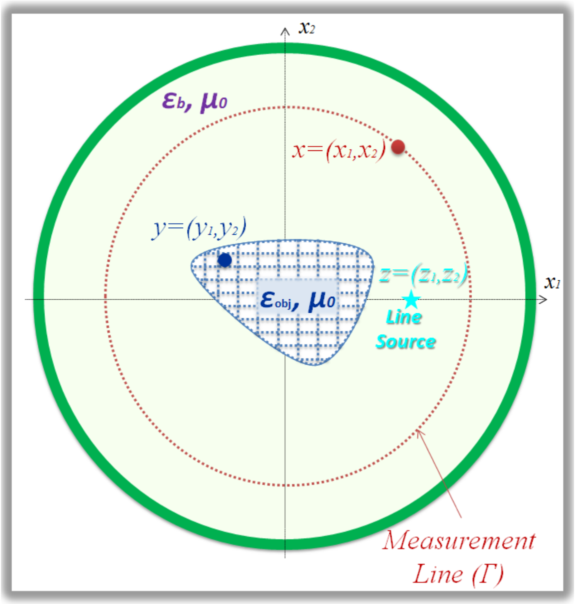

Figure 2.2 : Visualization of DE's parameters.

$$u^{s}(x;y) = i\left(\frac{\pi k_b}{2}\right)\sum_{n=1}^{N}(\varepsilon_{n_{obj}} - 1)u_n a_n J_1(k_b a_n)H_0^{(1)}(k_b\rho_n) - \frac{ik^2}{4}\Delta x_1 \Delta x_2 \sum_{nn=-\infty}^{\infty}\frac{H_{nn}^{(1)}(k_b a)}{J_{nn}(k_b a)}J_{nn}(k_b\rho')J_{nn}(k_b\rho)e^{inn(\phi-\phi')}\sum_{n=1}^{N}(\varepsilon_{n_{obj}} - 1)u_n \tag{2.20}$$

Lastly, it is better to mention form of incidence field. It is also composed of free space and reflected terms. Equation **(2.21)** denotes incident field clearly.

$$u^{i}(y;z) = \frac{i}{4}H_0^{(1)}(k|\rho - \rho'|) - \frac{i}{4}\sum_{nn=-\infty}^{\infty}\frac{H_{nn}^{(1)}(ka)}{J_{nn}(ka)}J_{nn}(k\rho')J_{nn}(k\rho)e^{inn(\phi-\phi')} \tag{2.21}$$

2.3 Analytic Solution for A Special Case

Several geometries have both analytic and numeric solutions for total/scattered field computations. To ensure accuracy of moment method, analytic solution is also performed. Along this section, analytic solution of closed mediums having PEC borders will be explained.

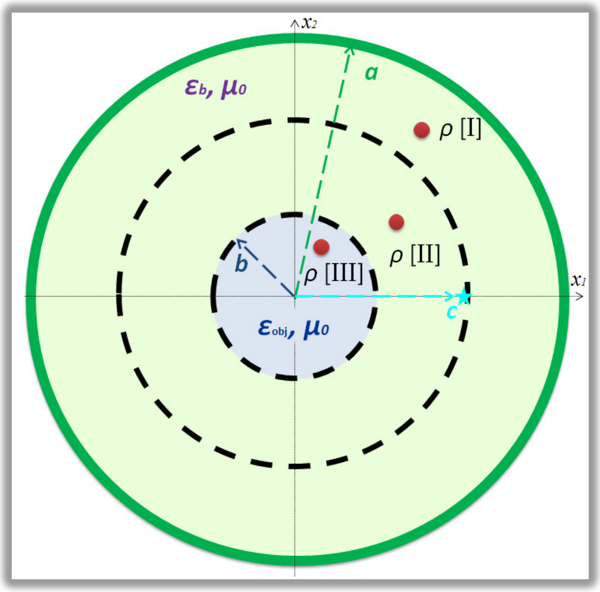

Figure 2.3 : The scattering problem from dielectric circular cylinder and possible positions for an observer.

The scattering problem from dielectric circular cylinder radius of *"b"* and three regions according to position of observation are visualized in Figure 2.3. The first part represents the condition where observation is greater than source *"c"* and bounded by PEC enclosure having a radius of *"a"*. The second one concerns radius of observer is greater object but less than source. For these two regions, both incident and reflected fields are involved. Therefore, Bessel and Hankel functions of first kind are used to define total field denoted by *"u"*. Finally, for the observations inside the dielectric only reflected fields (Bessel functions of first kind) are taken into account. The combination of three region definitions is inserted to infinite summation by using Fourier series expansion.

$$\hat{u}(\rho,n;\rho',\phi')=\begin{cases} A_n H_n^{(1)}(k_b\rho)+B_n J_n(k_b\rho) & , \quad c\le\rho\le a \quad [\mathrm{I}] \\ C_n H_n^{(1)}(k_b\rho)+D_n J_n(k_b\rho) & , \quad b\le\rho\le c \quad [\mathrm{II}] \\ E_n J_n(k_{obj}\rho) & , \quad 0\le\rho\le b \quad [\mathrm{III}] \end{cases} \tag{2.22}$$

Applying Fourier series expansion, we obtained:

$$u(\rho,\phi;\rho',\phi')=\frac{1}{2\pi}\sum_{n=-\infty}^{\infty}\hat{u}(\rho,n;\rho',\phi')e^{in\phi} \tag{2.23}$$

It is better to remind that source is located at distance *"c"* and its incidence angle is zero. Total field can be denoted as follows:

$$u(\rho,\phi;c,0)=\begin{cases}\dfrac{1}{2\pi}\displaystyle\sum_{n=-\infty}^{\infty}\left[A_nH_n^{(1)}(k_b\rho)+B_nJ_n(k_b\rho)\right]e^{in\phi} & , \ c\le\rho\le a\\ \dfrac{1}{2\pi}\displaystyle\sum_{n=-\infty}^{\infty}\left[C_nH_n^{(1)}(k_b\rho)+D_nJ_n(k_b\rho)\right]e^{in\phi} & , \ b\le\rho\le c\\ \dfrac{1}{2\pi}\displaystyle\sum_{n=-\infty}^{\infty}E_nJ_n(k_{obj}\rho)e^{in\phi} & , \ 0\le\rho\le b\end{cases} \tag{2.24}$$

There are five equations with five unknowns. It is required to written down matching and boundary conditions (BCs). Matching conditions are relevant to source point *"c"*. On the other hand, BCs are can be written in PEC and dielectric boundaries thanks to continuity of electric and magnetic field components.

$$u(\rho=c+0)-u(\rho=c-0)=0 \tag{2.25a}$$

$$\frac{\partial u}{\partial\rho}(\rho=c+0)-\frac{\partial u}{\partial\rho}(\rho=c-0)=\frac{-1}{c}e^{-in0}\bigg|_{\rho=c}=\frac{-1}{c} \tag{2.25b}$$

$$u(\rho=a-0)=0 \tag{2.25c}$$

$$u(\rho=b+0)-u(\rho=b-0)=0 \tag{2.25d}$$

$$\frac{\partial u}{\partial\rho}(\rho=b+0)-\frac{\partial u}{\partial\rho}(\rho=b-0)=0 \tag{2.25e}$$

The coefficients of infinite summations are found via Equations **(2.22)** and **(2.25a-e)**.

$$A_n=\frac{C_nH_n^{(1)}(k_bc)+D_nJ_n(k_bc)}{[SS]} \tag{2.26a}$$

$$B_n=-A_n[TT] \tag{2.26b}$$

$$C_n=\frac{-\dfrac{i\pi}{2}[SS]\left[k_bJ_n^{'}(k_bb)-k_{obj}\dfrac{J_n(k_bb)}{J_n(k_{obj}b)}J_n^{'}(k_{obj}b)\right]}{k_b\left[H_n^{'(1)}(k_bb)-[TT]J_n^{'}(k_bb)\right]+k_{obj}\dfrac{J_n^{'}(k_{obj}b)}{J_n(k_{obj}b)}\left[-H_n^{(1)}(k_bb)+J_n(k_bb)[TT]\right]} \tag{2.26c}$$

$$D_n = -C_n[TT] + \frac{i\pi}{2}\left[SS\right] \tag{2.26d}$$

$$E_n = \frac{\left[C_n H_n^{(1)}(k_b b) + D_n J_n(k_b b)\right]}{J_n(k_{obj} b)} \tag{2.26e}$$

$$where \quad TT \quad \frac{H_n^{(1)}(k_b a)}{J_n(k_b a)} \quad , \quad SS \quad \left[H_n^{(1)}(k_b c) - [TT] J_n(k_b c)\right]$$

These coefficients are inserted to Equation **(2.24)** and total field is calculated. However, our interest is scattered field. Since total field is composed of incident and reflected parts, if incident field is found then scattered one is acquired as well. 2D line source is applied as a source injection. Therefore, incident field remains same as Equation **(2.21)**.

3. INVERSE PROBLEM

Inverse scattering problems aim to investigate the location, geometry and physical properties of scatterers under the assumption of known scattered field. Thus, the steps of acquiring scattered field is expressed in previous section in depth. In this section, using measured scattered field, object profile will be obtained. For this reason, it is needed to define a new domain called by reconstruction that is likely to contain scatterers. Various strategies are developed to approach inverse scattering problems such as first-order Born Approximation, Rytov Approximation, extended Born, Newton, CSI and MR-CSI. Inverse scattering problem for a closed medium is first solved with a Born Approximation method that is valid for some special restrictions are satisfied. Then, a more general method named by Newton is employed. Multi-source effects on these two method are also clarified.

3.1 Born Approximation

Born Approximation (BA) shows good performance if the sought objects are weak scatterers [20]. In this way, total field in integral equation can be replaced by incident one, because scattered field is small enough to ignore. This restriction can be stated as follows:

$$\left\| k_0^2 \upsilon \right\| \quad 1 \tag{3.1}$$

Eq. **(3.1)** shows that if operating frequency and/or object function is low then BA method works well.

3.1.1 Born approximation procedure

In order to apply an inversion algorithm, one should write down scattered field formula in terms of reconstruction domain.

$$u^s(x) = k_b^2 \int_\Omega g(x,y)\upsilon(y)u(y)dy \quad where\ x \in \Gamma\ and\ dy = dy_1 dy_2 \tag{3.2}$$

The reconstruction area *"Ω"* must be selected wide enough, since sought object must be included. *"$u^s(x)$"* is scattered field in observation line *"Γ"*. *"$\upsilon(y)$"* is object function in reconstruction domain . When low-contrast scatterers are taken into account, total field approximates incident field in Eq. **(3.2)** according to BA.

$$u^s(x) = k_b^2 \int_\Omega g(x,y)\upsilon(y)u^i(y)dy \quad where\ x \in \Gamma\ and\ dy = dy_1 dy_2 \tag{3.3}$$

To solve *"υ"*, reconstruction area is divided into *"N"* small segments like forward problem solution and incident field is constant over a cell. By this means, both object function *"υ"* and incident field *"u^i"* can be extracted from integration. Now it is easy to integrate Eq. **(3.3)**. The only difference from MoM solution is that of *"y"* are the points placed in reconstruction domain.

$$u^s(x) = k_b^2 \sum_{n=1}^{N} \upsilon(y_n) u^i(y_n) \int_{D_n} g(x,y_n)dy_n \tag{3.4}$$

It can be seen from Eq. **(3.4)**, scattered field on observer line is transformed form of object function *"υ"*. Thus, unknown object function can be determined through applying linear algebra technique.

$$T\upsilon = u^s \qquad \Rightarrow \qquad \upsilon = T^{-1}u^s \tag{3.5}$$

"u^s" is *"Rx1"* matrix which is obtained via forward problem in *"R"* observation points. The size of *"T"* matrix is *"RxN"* because of reconstruction domain discretization. The entities of *"T"* are calculated by means of Eq. **(3.6)**.

$$T_{rn} = k_b^2 u^i(y_n) \int_{D_n} g(x_r, y_n)dy_n \quad where\ \ r = 1,2,...,R \tag{3.6}$$

Unfortunately, the solution for object function given in Eq. **(3.5)** is not enough to overcome our inverse problem. Since inverse of *"T"* matrix does not exist; and it causes ill posedness. This can be eliminated by variety of ways. Tikhonov regularization is one of them and used to handle ill posedness during this thesis.

$$\left(\alpha I + T^*T\right)\upsilon = T^*u^s \tag{3.7}$$

Tikhonov procedure starts with the multiplication by both sides by complex conjugate of *"T"* matrix. Then, a diagonal matrix is added to left side. The diagonal entities of this matrix are all identical and equal to *"α"* that is a very small number, zero for ideal case. Therefore, through Section 4 *"α"* is selected as much small as which do not cause an ill posedness again.

$$\upsilon = \left(\alpha I + T^{*}T\right)^{-1} T^{*}u^{s} \qquad \textbf{(3.8)}$$

3.1.2 Born approximation for multi-source case

Realizing small changes on BA procedure, one can attain better results. Multi-source injection to simulation area provides enhancement in shape reconstruction, so Eq. **(3.4)** is revised a bit.

$$u^{s}(x_r, z_q) = k_b^2 \sum_{n=1}^{N} \upsilon(y_n) u^{i}(y_n, z_q) \int_{D_n} g(x_r, y_n) dy_n \quad \text{where } q = 1,2,\ldots,Q \qquad \textbf{(3.9)}$$

The supplementary term *"* z_q *"* defines source points that are valued from *1* to *"Q"*. Besides, it is worth noting that forward problem solution must be also revisited. It is seen from the left side of Equation **(3.9)**.

The computation of entities of *"T"* matrix is now altered to:

$$T_{(r,q)n} = k_b^2 u^{i}(y_n, z_q) \int_{D_n} g(x_r, y_n) dy_n \quad \text{where } q = 1,2,\ldots,Q \qquad \textbf{(3.10)}$$

The size of *"T"* matrix is now *"(RxQ)xN"*. Extra rows are inserted to *"T"* matrix due to *"Q"* source points. The effect of one source on *"R"* observation results in *"R"* rows. It means effect of *"Q"* sources on *"R"* observation give rise to *"RxQ"* rows. *"T"* matrix can be represented clearly as follow:

$$T=\begin{bmatrix} k_b^2u^i(y_1,z_1)\int_{D_1}g(x_1,y_1)dy_1 & k_b^2u^i(y_2,z_1)\int_{D_2}g(x_1,y_2)dy_2 & \dots & k_b^2u^i(y_N,z_1)\int_{D_N}g(x_1,y_N)dy_N \\ k_b^2u^i(y_1,z_1)\int_{D_1}g(x_2,y_1)dy_1 & k_b^2u^i(y_2,z_1)\int_{D_2}g(x_2,y_2)dy_2 & \dots & k_b^2u^i(y_N,z_1)\int_{D_N}g(x_2,y_N)dy_N \\ \dots & & & \\ k_b^2u^i(y_1,z_1)\int_{D_1}g(x_R,y_1)dy_1 & k_b^2u^i(y_2,z_1)\int_{D_2}g(x_R,y_2)dy_2 & \dots & k_b^2u^i(y_N,z_1)\int_{D_N}g(x_R,y_N)dy_N \\ k_b^2u^i(y_1,z_2)\int_{D_1}g(x_1,y_1)dy_1 & k_b^2u^i(y_2,z_2)\int_{D_2}g(x_1,y_2)dy_2 & \dots & k_b^2u^i(y_N,z_2)\int_{D_N}g(x_1,y_N)dy_N \\ \dots & & & \\ k_b^2u^i(y_1,z_Q)\int_{D_1}g(x_R,y_1)dy_1 & k_b^2u^i(y_2,z_Q)\int_{D_2}g(x_R,y_2)dy_2 & \dots & k_b^2u^i(y_N,z_Q)\int_{D_N}g(x_R,y_N)dy_N \end{bmatrix}$$

Even if multi-source technique is carried out, ill posedness of the problem remains. Same procedure as single source is performed in Eq. **(3.8)**.

3.1.3 Born approximation - closed and unbounded medium

The solely difference between closed and unbounded medium for BA method is integration of Green's function. In the solution of inverse problem requires finding of *"T"* matrix as it is expressed in previous section.

Firstly, let us remind to Green's function *"g_c"* of closed medium.

$$g_c(\rho,\phi;\rho',\phi')=\frac{i}{4}H_0^{(1)}(k_b|\rho-\rho'|) -\frac{i}{4}\sum_{nn=-\infty}^{\infty}\frac{H_{nn}^{(1)}(k_ba)}{J_nn(k_ba)}J_{nn}(k_b\rho')J_{nn}(k_b\rho)e^{inn(\phi-\phi')}\ ,\quad 0\le\rho\le a \qquad \textbf{(3.11)}$$

The calculation of *"T"* matrix entities is given in Eq. **(3.12)**. There is no singularity between observers and sources. Thus, taking an integral over a small cell of reconstruction domain is enough. *"T^c "* matrix can be found as:

$$\begin{aligned} T_{rn}^c &= (\Delta x\Delta y)k_b^2 \\ &\cdot\left[\frac{i}{4}H_0^{(1)}(k_b|y_n-z_q|)-\frac{i}{4}\sum_{nn=-\infty}^{\infty}\frac{H_{nn}^{(1)}(k_ba)}{J_{nn}(k_ba)}J_{nn}(k_bz_q)J_{nn}(k_by_n)e^{inn(\phi_{y_n}-\phi_{z_q})}\right] \\ &\cdot\left[\frac{i}{4}H_0^{(1)}(k_b|x_r-y_n|)-\frac{i}{4}\sum_{nn=-\infty}^{\infty}\frac{H_{nn}^{(1)}(k_ba)}{J_{nn}(k_ba)}J_{nn}(k_bx_r)J_{nn}(k_by_n)e^{inn(\phi_{x_r}-\phi_{y_n})}\right] \end{aligned} \qquad \textbf{(3.12)}$$

On the other hand, for unbounded medium Green's function *"g_u"* is expressed as:

$$g_u(\rho,\rho') = \frac{i}{4} H_0^{(1)}(k|\rho - \rho'|) \qquad 0 \le \rho \le \infty \tag{3.13}$$

Now, the computation of *"T^u"* matrix is revised:

$$T^u_{rn} = (\Delta x \Delta y) k_b^2 \left(\frac{i}{4} H_0^{(1)}(k_b |y_n - z_q|) \right) \left(\frac{i}{4} H_0^{(1)}(k_b |x_r - y_n|) \right) \tag{3.14}$$

The rest of the formulations are same for two cases PEC enclosure exists or not.

3.2 Newton Method

Newton method can be applied to high or low contrast objects without any limitation, so it is a more general approach when compared to Born Approximation. It requires a prediction of object function at first. Then, it aims to reach or get closer the exact value of object function. There is no restriction for operating frequency or physical property of sought object.

3.2.1 Newton procedure

The scattered field was demonstrated before thanks to DE. Let us go further one more step. The right side of DE points out that an operator *"F"* applied to object function *"υ"*, so the left side of DE is altered. In addition, interested area is now reconstruction domain *"Ω"*.

$$F(\upsilon) = k_b^2 \int_\Omega g(x,y)\upsilon(y)u(y)dy \quad where\ x \in \Gamma\ and\ dy = dy_1 dy_2 \tag{3.15}$$

The predicted initial value of object function *"$\upsilon^{(0)}$"* and Fréchet derivative allows us to linearize the Equation **(3.15)**.

$$F(\upsilon^{(0)}) + F'(\upsilon^{(0)})\delta\upsilon^{(1)} = u^s \tag{3.16}$$

"$F(\upsilon^{(0)})$" is a solution of Eq. **(3.15)** under the condition of estimated object function. There is only one unknown term *"$u^{(0)}$"* that is an initial value for total field. The computations done for *"$u^{(0)}$"* are almost identical to MoM procedure in forward problem solution. Now, the reconstruction is divided into *"N"* small pieces where

total field over a cell be constant. To achieve, entities of *"A"* matrix should be calculated regarding reconstruction area. "x_m"s are the center points of a *"D_n"* cell.

$$A_{mn} = k_b^2 \upsilon_n^{(0)} \int_{D_n} g(x_m, y_n) dy \quad where\, m = 1,2,...,N \tag{3.17}$$

Under the condition of known incident field "u^i", total field can be found via Eq. **(3.18)**.

$$\sum_{n=1}^{N} A_{mn} u_n^{(0)} = u_m^i \quad where\, m = 1,2,...,N \tag{3.18}$$

Furthermore, Fréchet derivative should be explored. According to its definition, it can be expressed as:

$$F'(\upsilon^{(0)})\delta\upsilon^{(1)} \quad k_b^2 \int_{\Omega} g(x,y) u^{(0)}(y) \delta\upsilon^{(1)} dy \tag{3.19}$$

Equation **(3.19)** is inserted to Eq. **(3.16)** and the Fréchet derivative is placed alone in the left side. Here, "u^s" is scattered field data in observation points.

$$k_b^2 \int_{\Omega} g(x,y) u^{(0)}(y) \delta\upsilon^{(1)} dy = u^s - F(\upsilon^{(0)}) \tag{3.20}$$

Eq. **(3.20)** is now represented as a system of linear equations. There is a new matrix *"B"* sizes *"RxN"*. *"R"* is the number of observation points. Besides, "$\delta\upsilon^{(1)}$" is *"Nx1"* matrix over a reconstruction domain.

$$B_{rn} = k_b^2 \int_{\Omega_n} g(x_r, y_n) u^{(0)}(y_n) dy \quad where\, r = 1,2,...,R \tag{3.21}$$

The only step is necessary to be performed is solving Eq. **(3.20)** for "$\delta\upsilon^{(1)}$". Unfortunately, ill posedness arises again. To cope with ill-conditioned problem, Tikhonov regularization method is revisited.

$$B\delta\upsilon^{(1)} = [u^s - F(\upsilon^{(0)})] \quad \Rightarrow \quad \left(\alpha I + B^* B\right)\delta\upsilon^{(1)} = B^*[u^s - F(\upsilon^{(0)})] \tag{3.22}$$

"$\delta\upsilon^{(1)}$" is found via applying inverse of additional term for two sides. It is finalize in Eqn. **(3.23)**.

$$\delta\upsilon^{(1)} = \left(\alpha I + B^{*}B\right)^{-1} B^{*}[u^{s} - F(\upsilon^{(0)})] \tag{3.23}$$

It is mentioned that Newton method is an iterative approach, so predicted object function should be updated. It is achieved by performing Eq. **(3.24)**.

$$\upsilon^{(1)} = \upsilon^{(0)} + \delta\upsilon^{(1)} \tag{3.24}$$

At the end of n^{th} iteration step, Eq. **(2.24)** can be expressed as in general.

$$\upsilon^{(n)} = \upsilon^{(n-1)} + \delta\upsilon^{(n)} \tag{3.25}$$

3.2.2 Newton method for multi-source case

The success of multi-source illumination is explained before. Like BA method, formulation of scattered field is modified. Not only scattered but also total field over a small cell are affected.

$$\sum_{n=1}^{N} A_{mn} u_{n}^{(0)}(y_{n}, z_{q}) = u_{m}^{i}(y_{n}, z_{q}) \quad where\ m = 1, 2, ..., N \tag{3.26}$$

where *"z_q"* shows source point that changes from 1 to *"Q"*. Total field over a cell is computed using Eqn. **(3.26)**. After that, to find Fréchet derivative *"B"* matrix should be expressed in terms of multi-sources.

$$B_{(r,q)n} = k_{b}^{2} \int_{D_{\Omega}} g(x_{r}, y_{n}) u^{(0)}(y_{n}, z_{q}) dy_{n} \quad where\ r = 1, 2, ..., R \tag{3.27}$$

Size of *"B"* matrix is expanded to *"(RxQ)xN"*. For each source, new rows are added to *"B"* matrix.

$$B = \begin{bmatrix} k_b^2\int_{D_1} g(x_1,y_1)u^{(0)}(y_1,z_1)dy_1 & k_b^2\int_{D_2} g(x_1,y_2)u^{(0)}(y_2,z_1)dy_2 & \ldots & k_b^2\int_{D_N} g(x_1,y_N)u^{(0)}(y_N,z_1)dy_N \\ k_b^2\int_{D_1} g(x_2,y_1)u^{(0)}(y_1,z_1)dy_1 & k_b^2\int_{D_2} g(x_2,y_2)u^{(0)}(y_2,z_1)dy_2 & \ldots & k_b^2\int_{D_N} g(x_N,y_N)u^{(0)}(y_N,z_1)dy_N \\ \ldots & & & \\ k_b^2\int_{D_1} g(x_R,y_1)u^{(0)}(y_1,z_1)dy_1 & k_b^2\int_{D_2} g(x_R,y_2)u^{(0)}(y_2,z_1)dy_2 & \ldots & k_b^2\int_{D_N} g(x_R,y_N)u^{(0)}(y_N,z_1)dy_N \\ k_b^2\int_{D_1} g(x_1,y_1)u^{(0)}(y_1,z_2)dy_1 & k_b^2\int_{D_2} g(x_1,y_2)u^{(0)}(y_2,z_2)dy_2 & \ldots & k_b^2\int_{D_N} g(x_1,y_N)u^{(0)}(y_N,z_2)dy_N \\ \ldots & & & \\ k_b^2\int_{D_1} g(x_R,y_1)u^{(0)}(y_1,z_Q)dy_1 & k_b^2\int_{D_2} g(x_R,y_2)u^{(0)}(y_2,z_Q)dy_2 & \ldots & k_b^2\int_{D_N} g(x_R,y_N)u^{(0)}(y_N,z_Q)dy_N \end{bmatrix}$$

Multi-source injection cannot overcome ill posedness, so identical Tikhonov solution is an easy way to handle.

3.2.3 Newton method - closed vs. unbounded medium

For different mediums, GF definition varies as it was said. GF for closed and unbounded mediums are given in Section 2. Entities of *"B"* matrix are influenced by these definitions. *"B"* matrix is given below for both mediums separately. *"* B^c *"* is related to closed medium, whereas *"* B^u *"* is relevant to unbounded one.

$$\begin{aligned} B^c_{rn} &= (\Delta x \Delta y)k_b^2 \\ &.\left[\frac{i}{4}H_0^{(1)}(k_b|x_r - y_n|) - \frac{i}{4}\sum_{nn=-\infty}^{\infty}\frac{H_{nn}^{(1)}(k_b a)}{J_{nn}(k_b a)}J_{nn}(k_b x_r)J_{nn}(k_b y_n)e^{inn(\phi_{x_r}-\phi_{y_n})}\right] \\ &.\ u^{(0)}(y_n) \\ &= (\Delta x \Delta y)k_b^2 \\ &.\left[\frac{i}{4}H_0^{(1)}(k_b|x_r - y_n|) - \frac{i}{4}\sum_{nn=-\infty}^{\infty}\frac{H_{nn}^{(1)}(k_b a)}{J_{nn}(k_b a)}J_{nn}(k_b x_r)J_{nn}(k_b y_n)e^{inn(\phi_{x_r}-\phi_{y_n})}\right] \\ &.\ A^{-1}\left[\frac{i}{4}H_0^{(1)}(k_b|y_n - z|) - \frac{i}{4}\sum_{nn=-\infty}^{\infty}\frac{H_{nn}^{(1)}(k_b a)}{J_{nn}(k_b a)}J_{nn}(k_b z)J_{nn}(k_b y_n)e^{inn(\phi_{y_n}-\phi_{z})}\right] \end{aligned} \quad \textbf{(3.28)}$$

$$\begin{aligned} B^u_{rn} &= (\Delta x \Delta y)k_0^2\left(\frac{i}{4}H_0^{(1)}(k|x_r - y_n|)\right)u^{(0)}(y_n) \\ &= (\Delta x \Delta y)k_0^2\left(\frac{i}{4}H_0^{(1)}(k|x_r - y_n|)\right)A^{-1}\left(\frac{i}{4}H_0^{(1)}(k|y_n - z|)\right) \end{aligned} \quad \textbf{(3.29)}$$

The rest of the computations is same for two cases PEC enclosure remains or not.

4. NUMERICAL RESULTS

In this section, a variety of numerical applications are carried out to test accuracy, performance and utilities of PEC surroundings for inverse scattering problems related to arbitrary objects. Not only closed but also unbounded mediums are taken into account. The differences and similarities between the results of these configurations are examined. We mainly aimed to explore geometry, location and physical properties of lossless dielectric objects buried in closed medium. The formulations presented in Section 3 enable us to achieve it. Another vital objective that is verification of forward problem solution is also satisfied through Section 2.

This section involves four subheadings. Primarily, Green's functions of closed and unbounded mediums are analyzed. The similar outcomes in Ref. [13] are attained. Secondly, the forward problem solution of moment method is verified owing to analytic solution for closed mediums. Then, various examples are done to check the advantages of closed medium with respect to unbounded one if possible. These examples may comprise of several inhomogeneous scatterers instead of a single dielectric circular/rectangular one. Born Approximation and Newton methods are used in turn. Moreover, single vs. multi source comparisons are practiced.

Lastly, Crocco and Litman (2009) published a paper about design issues related to embedded microwave systems. To get better results for closed and unbounded mediums, the importance of simulation parameters' selection is mentioned there. During this thesis, we followed their suggestions in some cases.

4.1 Green's Function for Closed and Unbounded Mediums

Green's Function for closed medium is formulated in Section 2.1. Here, the magnitude of GF over a rectangular area is plotted. At *1 GHz*, a *10-cm^2* cross-section is considered inside a circular PEC enclosure of radius *20 cm* (see Fig. 4.1). PEC cylinder is filled a lossless background of $\varepsilon_b = 3$. A line source is applied at a point of *7.5 cm* from origin in x-direction. *2500* observation points are placed to *10-cm^2*

square. Most parameters are identical to Ref [13], but some information is not available. Therefore, we had to make up for missing parts such as the number of observers.

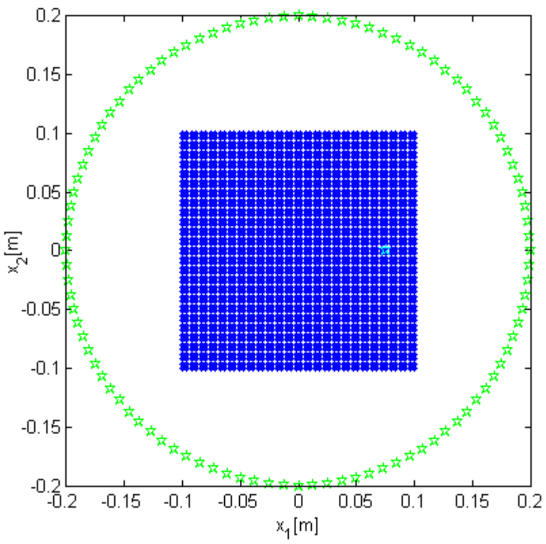

Figure 4.1 : A configuration for Green's Function comparison between closed and unbounded mediums [13].

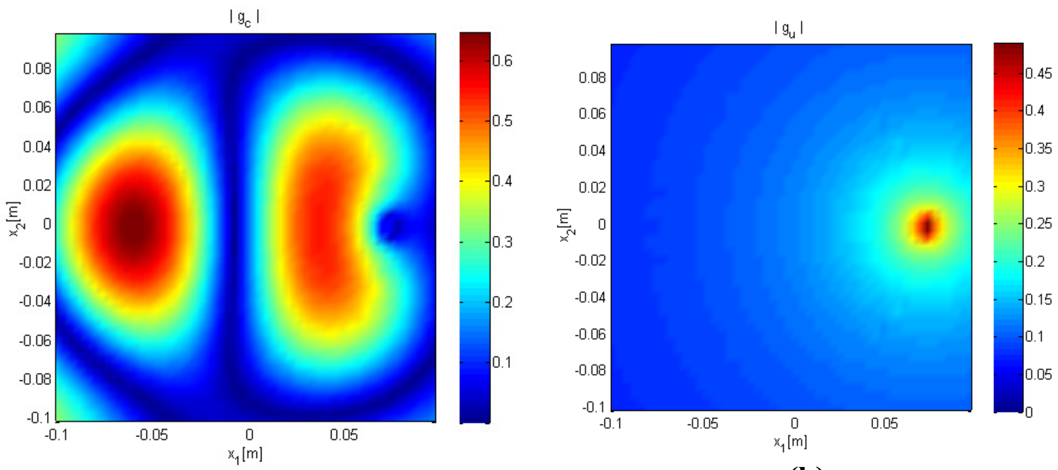

(a) **(b)**

Figure 4.2 : Green's Function over a *10-cm2* cross section for (a) closed medium (b) in the absence of PEC cylinder.

Figure 4.2 shows Green's function for closed and unbounded mediums. In unbounded case, Green's function is expressed as:

$$G(\rho,\rho') = \frac{i}{4} H_0^{(1)}(k|\rho - \rho'|) \quad 0 \le \rho \le \infty \tag{4.1}$$

The results in Fig. 4.2 (b) seems to be like [13], but (a) is quite different. It can be caused by the locations of observation points or limits of infinite series in GF formula. As it can also be seen from Fig. 4.2, closed medium has greater energy than unbounded one. Both forms have singular values at the source point. These two are also supported by [13,14].

4.2 A Verification of Scattered Field - Analytic vs. MoM

The accuracy of scattered field obtained from solution of forward problem is substantially crucial for collected synthetic data. Since, we must begin with an affirmation of our numeric results with analytic ones. There are few geometries have their own analytic solutions to compute scattered field. Analytic solution of circular dielectric cylinder exists and it is found in Section 2.3. On the other hand, Section 2.2 demonstrates method of moment solution of dielectric objects having an arbitrary shape.

Now, let us verify our formulations and coding. At *300 MHz*, a circular dielectric ($\varepsilon_{r_{obj}}=2$) radius of *30 cm* is put in free space. It is required to divide scatter into small pieces. For any object, even if the geometry is circular, rectangular meshing is implemented to eliminate singularities in moment procedure. The size of each cell is chosen as $\lambda/20$. A circular PEC enclosure radius of *1.4 m* surrounds the simulation area. A single line source is injected at a distance of *50 cm* from the origin. The incidence angle is $0°$. Three hundred and sixty observation points are placed on a circle radius of *70 cm*. A visualization of all mentioned stuff is drawn in Fig. 4.3.

Analytic method involves several infinite series summations for coefficient calculations. The limits of series are determined by observing total fields. We specified an interval where total field remain unchanged even if we alter the limits. In order to minimize simulation duration, the smallest value of interval is selected as a limit of series.

Analytic solution provides us total field directly. To obtain scattered one, incident fields must be extracted. Incident field is given in earlier sections. Therefore, simply subtracting incident one from total field ensures us scattered one. According to these explanations, absolute value of scattered & total fields vs. observation points is plotted analytically and numerically (see Fig. 4.4).

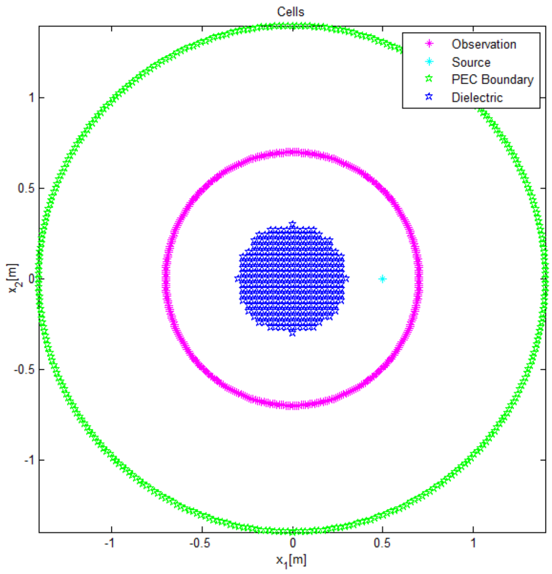

Figure 4.3 : A sample configuration.

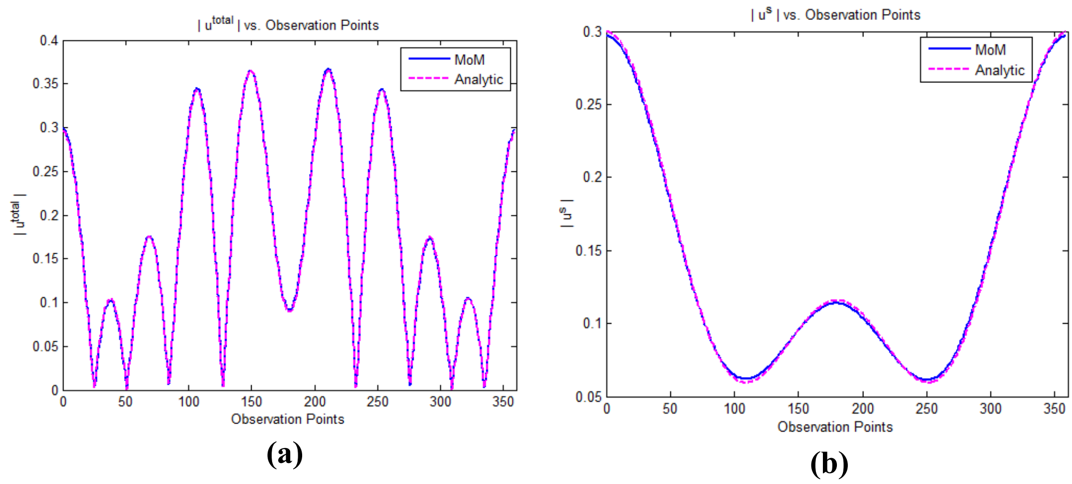

Figure 4.4 : Absolute of (a) Total field (b) Scattered field vs. observation points for an example visualized in Figure 4.3.

As we expected, maximum values of scattered field are found in some observers in front of a source. For a selected discretization (*λ/20* for each cell), analytic and numeric solutions agree well. By the way, limits of series is now *(-25,+25)*.

4.3 Born Approximation Results for Closed and Unbounded Mediums

Now, we are prepared to solve inverse problem using provided synthetic data. During this part, Born Approximation technique will be used as highlighted in the headings. First closed, then unbounded medium solutions will be tested and compared.

We start with a circular dielectric cylinder investigation in PEC enclosure radius of *1.45 m*. Forward solution is performed to get scattered field at *300 MHz*. A dielectric whose relative permittivity is *1.1* is divided into small segments. The size of each segment is *λ/25*. This scatterer is excited by a single line source from a point of *80 cm* and an angle of *0°*. Then scattered field is recorded in *40* observation points at *1 m* away from object. Next, size of reconstruction area is determined. Each side of this area is *80 cm* for first example (see Fig. 4.5). Then, Born method is carried out based on procedure steps in Section 3.1. In order to suppress ill-posedness of the problem, Tikhonov regularization is implemented using a scaling factor $(\alpha = 10^{-10})$.

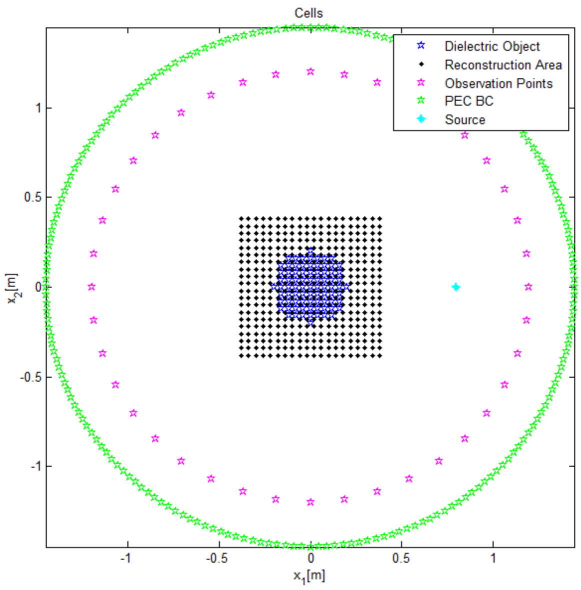

Figure 4.5 : First example with single line source for Born Approximation.

After a closed medium solution is done, we remove PEC surrounding and solve the problem in free space. This step will be done for all examples. Since there is no loss in scatterer, only real parts of the object function (contrast) function is plotted.

As it is acquired from Fig. 4.6, both solutions are good at finding the locations but not perfect at geometry and physical properties that must be *0.1* for object function.

As we claimed that multi source illumination can be helpful for us to attain better results. The only change from a previous example is increase in number of sources. Five transmitters are arranged in an order over a radius of *80 cm* in Figure 4.7. Here is an important point is that regularization parameter should be increased for closed medium solution $(\alpha = 10^{-3})$.

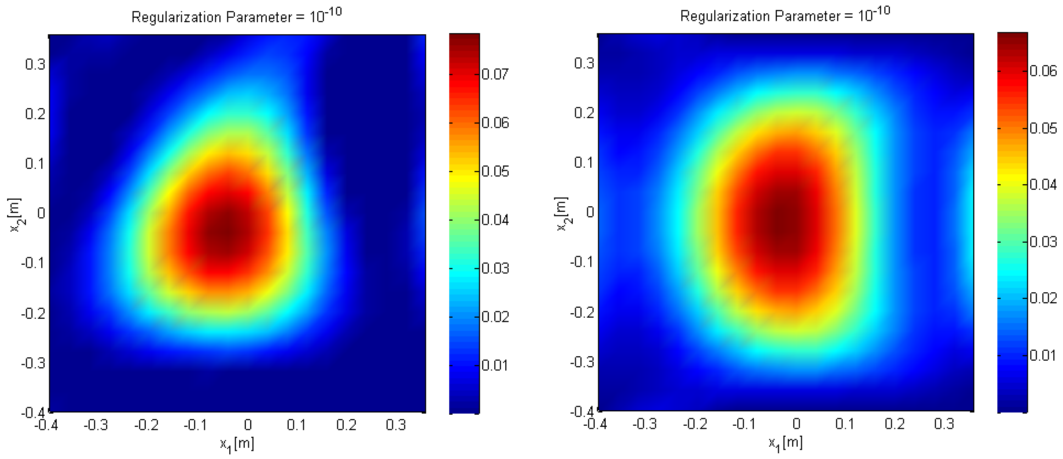

(a) **(b)**

Figure 4.6 : The real parts of object function attained using single line source for (a) closed (b) free space medium.

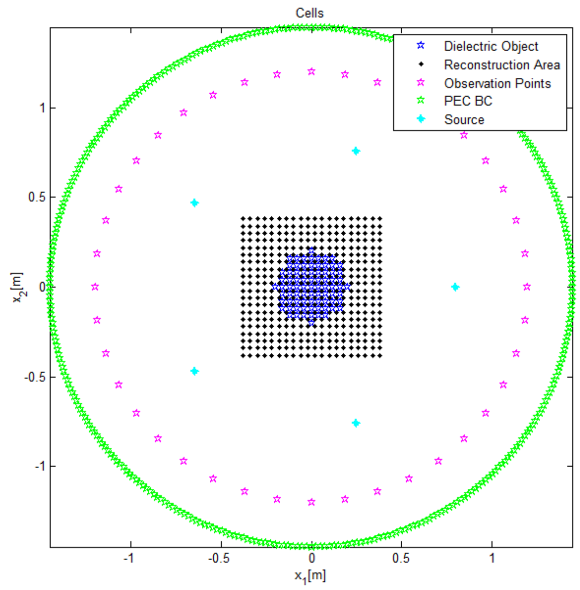

Figure 4.7 : An example with multi line source for Born Approximation.

The real parts of object function are plotted again in Figure 4.8. For both configurations, imaging is improved. The geometry and physical properties are now closed to real value. Hence, during this thesis we mainly prefer multi-source technique instead of a single one even if it lasts long period.

In first example, size of PEC enclosure is chosen randomly. At the beginning of this study, we were curious about impact of closure will enhance our reconstruction or not. Therefore, choice of surrounding radius was actually our main concern. We performed some examples and surprising outcomes are encountered. The results of most selections are acceptable. However, a few of them ruin inversion algorithm. At that point, we come across a paper [17].

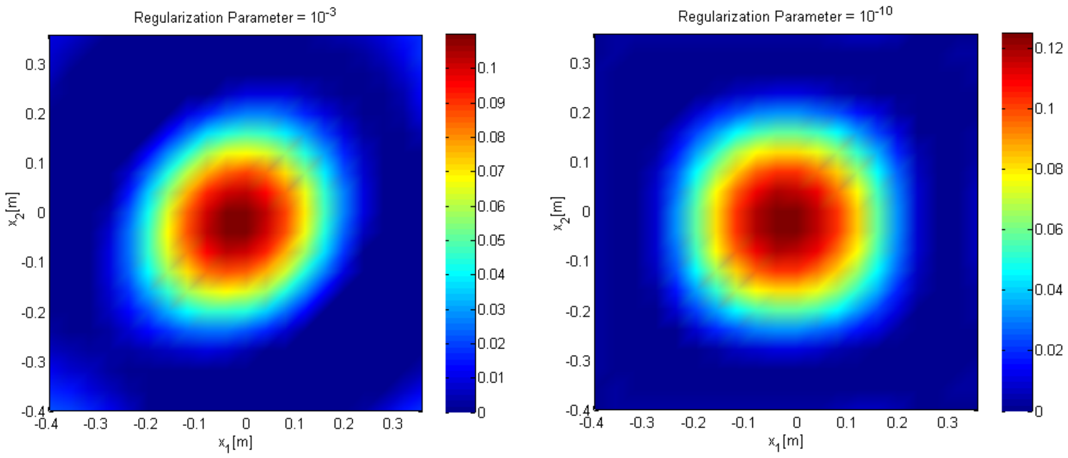

(a) **(b)**

Figure 4.8 : The real parts of object function attained using multi line source for (a) closed (b) free space medium.

Crocco and Litman claim that the distance between surrounding and observers is important. If the distance is *"λ/4"*, then it results in ideal circumstance while *"λ/2"* brings out a worst-case scenario. Following example is done to see the effect of radius of PEC enclosure.

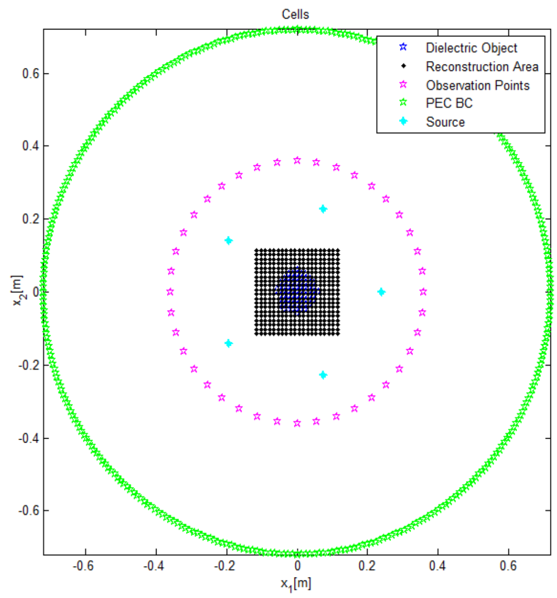

Figure 4.9 : A sample scenerio to observe effect of PEC radius.

At *1 GHz*, PEC cylinder radius of *72 cm (2.4λ)* surrounds a circular dielectric having a radius of *6 cm* and relative permittivity of *1.1*. Five line sources are used. Forty observers are aligned on a radius of *36 cm*. Now, the distance between observation and PEC surrounding $(\Delta_{\rho a})$ is *1.2λ*, which is arbitrarily selected. The real part of object function is demonstrated for closed and free space medium in Fig 4.10. Then, fixing all parameters except PEC radius simulations are performed repeatedly. In Fig.

4.10 (a) shows free space result and from (b) to (e) are related to closed one. The distance between observers and PEC surrounding is changed from 0.25λ to 3.80λ.

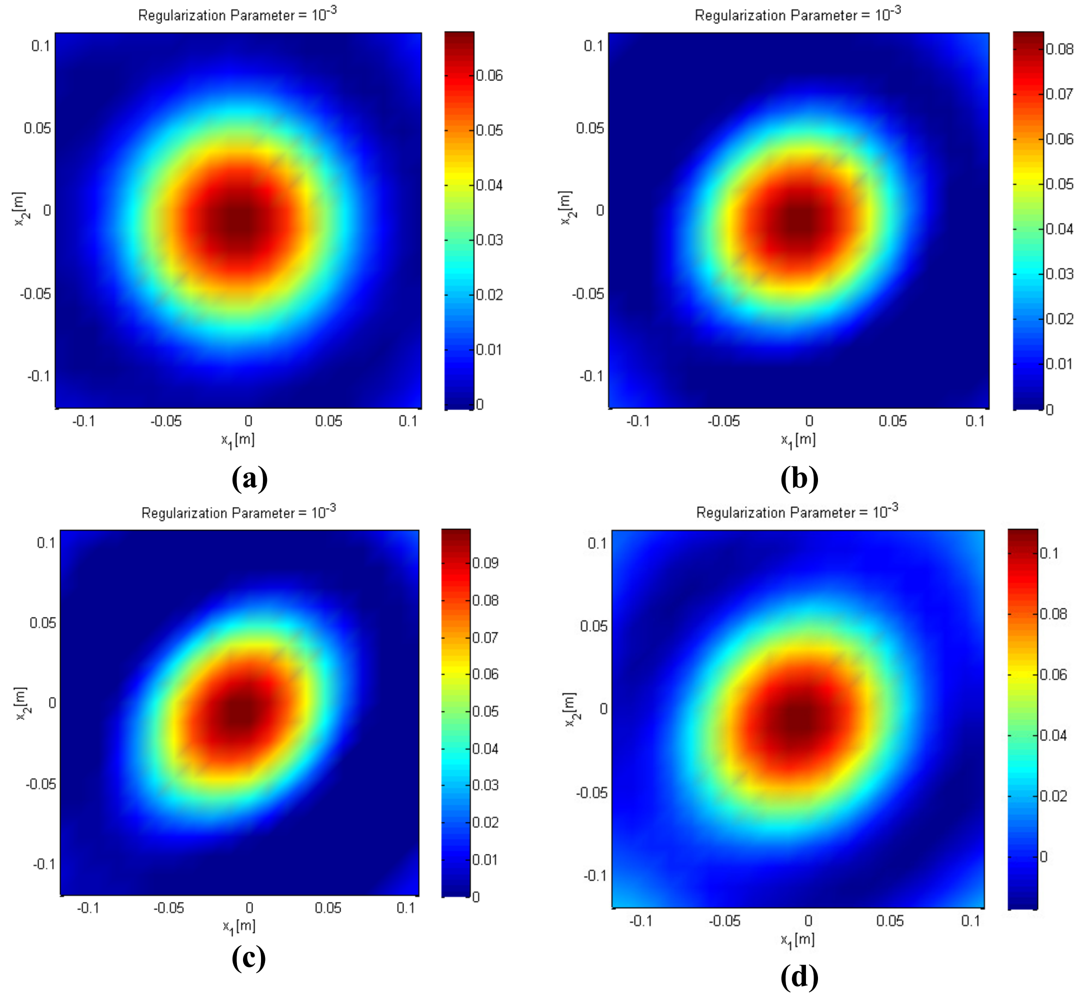

Figure 4.10 : The real parts of object function acquired for Fig. 4.9 (a) PEC is removed (b) $\Delta\rho a=1.2\lambda$ (c) $\Delta\rho a=3.8\lambda$ (d) $\Delta\rho a=0.25\lambda$ (e) $\Delta\rho a=0.5\lambda$.

Figure 4.10 promotes what we discussed in earlier. The best outcome for closed medium occurs when $\Delta_{\rho a}=0.25\lambda$ pictured in (d), whereas the worst one is shown up when $\Delta_{\rho a}=0.5\lambda$ drawn in (e). Although in (b) and (c) the contrast is lower than expected, determination of location and geometry is reasonable.

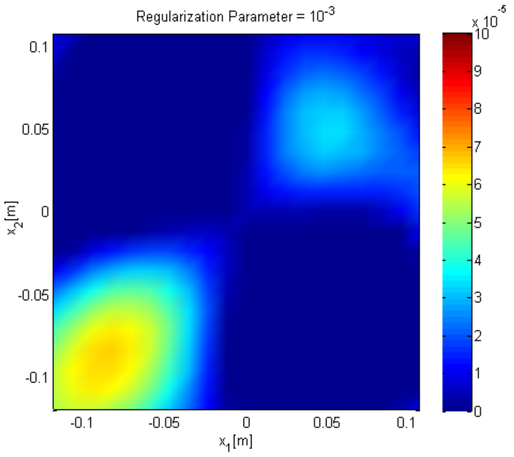

(e)

Figure 4.10 (cont.) : The real parts of object function acquired for Fig. 4.9 (a) PEC is removed (b) $\Delta\rho a=1.2\lambda$ (c) $\Delta\rho a=3.8\lambda$ (d) $\Delta\rho a=0.25\lambda$ (e) $\Delta\rho a=0.5\lambda$.

The size and location of reconstruction area is another issue that needs to be discussed. To test the effect of reconstruction size, a sample scenario is set up. At *1 GHz*, a circular dielectric ($\varepsilon_{r_{obj}}=1.1$) whose radius is *6 cm* is on center of simulation area. A conducting enclosure radius of *72 cm* surrounds the object. A single line source illuminates the object at a distance of *24 cm*. Its incident angle is *0*°. Forty observers are evenly located on a radius of *36 cm*. To apply an inversion algorithm, a *24 cm* sized rectangle is selected. This example is drawn in Fig. 4.11(a). Object profile reconstruction is realized when PEC enclosure exists and real part of object function is plotted in Fig. 4.12(a). Then, free space solution is done and real part of contrast is given in Fig. 4.12(b). As it is seen, both configurations locate the object and object profile is not bad. Next, reconstruction size is expanded to *36 cm*. All other parameters are fixed. The discretized cells of reconstruction area are quite close to observation points. It is pictured in Fig. 4.11(b). The results related to this example are given in Fig. 4.13.

When the distance between visionary radius of reconstruction area and observers ($\Delta_{r\rho}$) is decreased, free space solution is prominently affected. Its localization is reasonable, but object function is hugely deteriorated. In [17], size of reconstruction area is examined and it is stated that $\Delta_{r\rho}$ should be greater than 0.5λ for unbounded configurations. The value of $\Delta_{r\rho}$ is undesirable for Figure 4.13. Hence, defects in object function is indispensable.

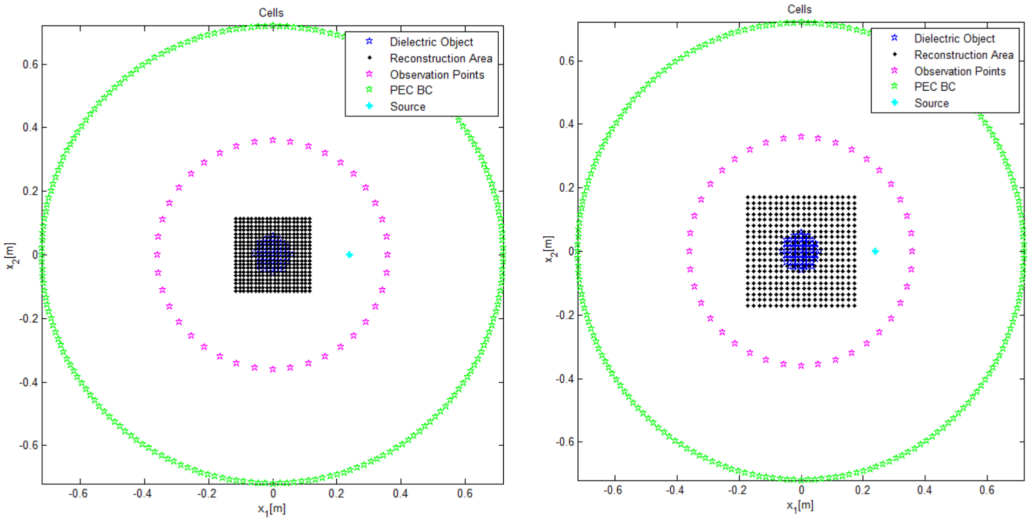

(a) **(b)**

Figure 4.11 : A sample scenerio to explore the effect of reconstruction size (a) *L*Ω *=24 cm*. (b) *L*Ω*=36 cm*.

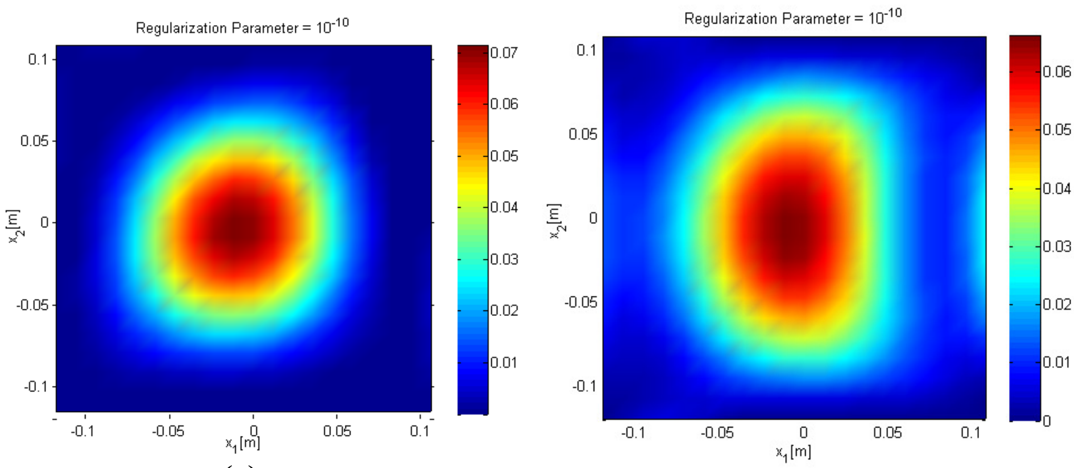

(a) **(b)**

Figure 4.12 : The real parts of object function attained when reconstruction size is *24 cm* for (a) closed (b) free space medium.

It is claimed that multi-scatterers can be reconstructed through our implementations. To observe performance of closed mediums, an example is performed. At *900 MHz*, two rectangular objects $(\varepsilon_{r_{obj}} = 1.2)$ in size of *10 cm* are put inside a PEC enclosure radius of *75 cm*. Forty observers are *0.25λ (8 cm)* far away from conducting boundary. Ten transmitters are located at a distance of *50 cm*. The reconstruction area is selected as *40 cm* for each side that possibly includes scatterers (see Figure 4.14).

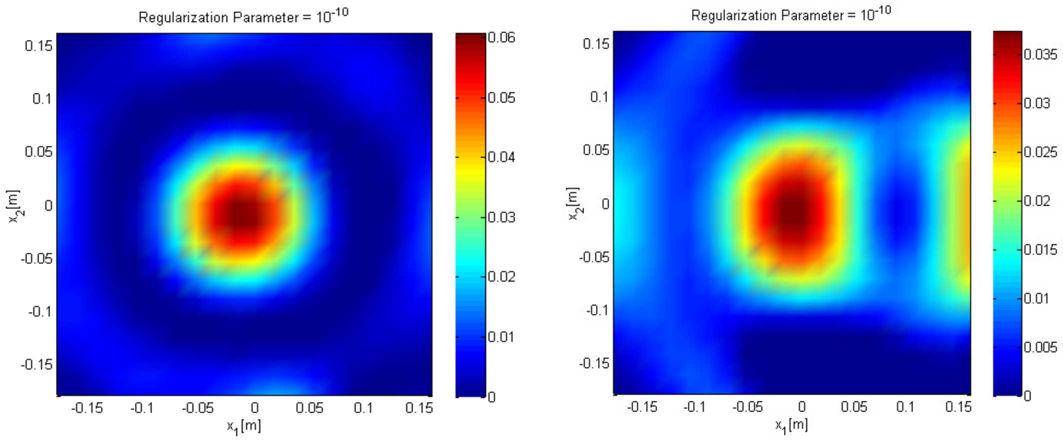

(a) **(b)**

Figure 4.13 : The real parts of object function attained when reconstruction size is *36 cm* for (a) closed (b) free space medium.

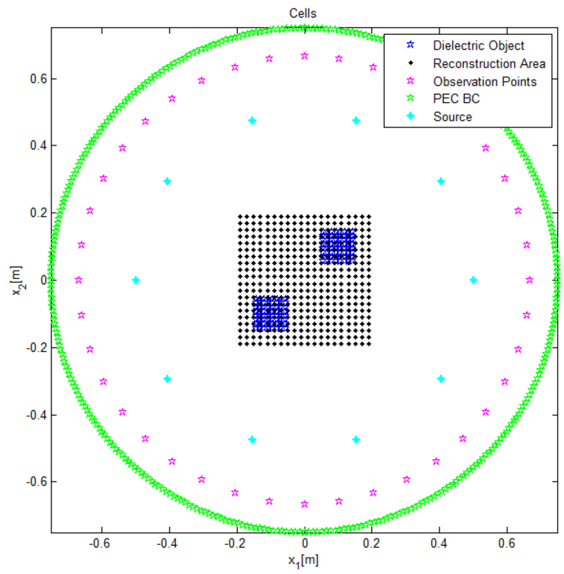

Figure 4.14 : An example involving two scatterers.

Both closed and free space solutions provide good conclusions for different regularization parameters. The regularization parameter α is set to *0.002* at first and results are given in Fig. 4.15. As it is observed, closed medium solution is quite well. The geometry, contrast and localization are found. However, contrast value for free space is not good enough as closed one to reconstruct the object profile.

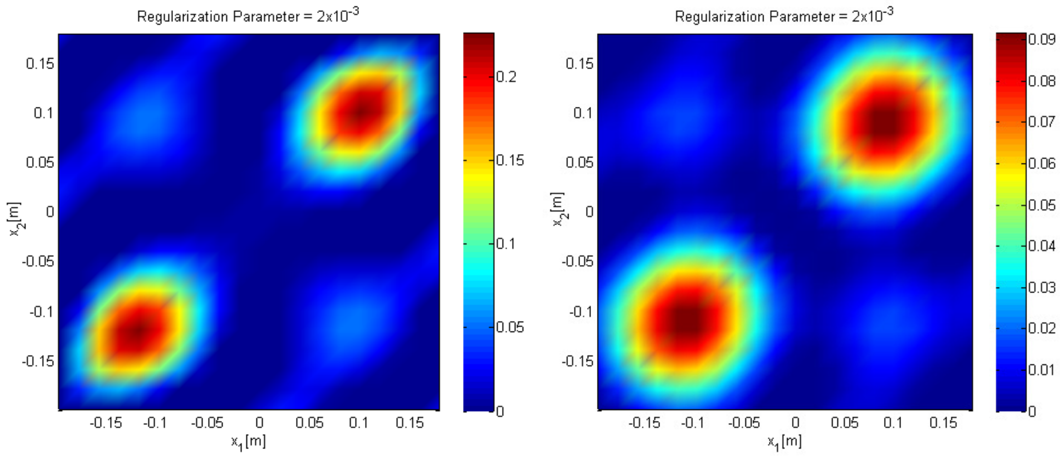

(a) **(b)**

Figure 4.15 : The real parts of object function acquired for (a) closed (b) free space medium includes two scatterers *(α=0.002)*.

Conversely, when α is changed to 10^{-4}, free space solution is apparently enhanced. These two configurations locate the objects in a better way, but an unexpected defect on contrast arises in closed medium.

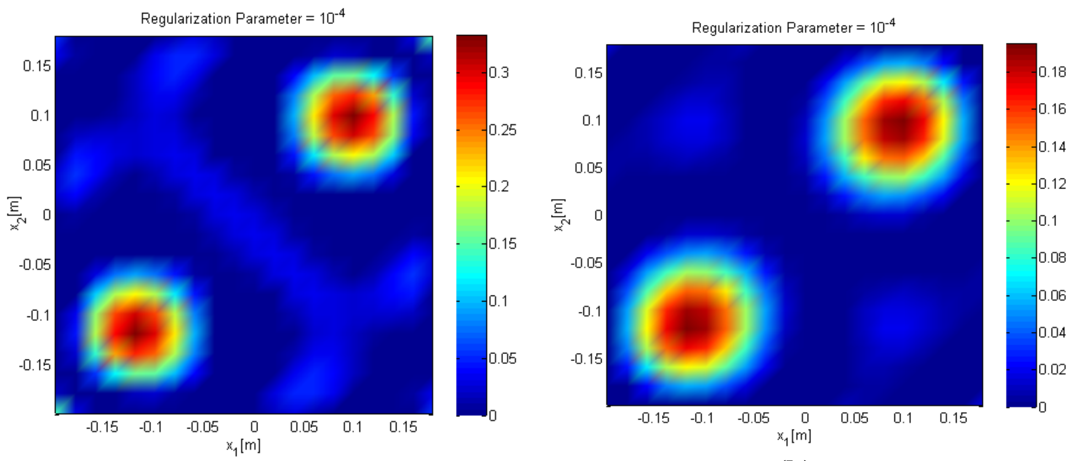

(a) **(b)**

Figure 4.16 : The real parts of object function acquired for (a) closed (b) free space medium includes two scatterers *(α=10^{-4})*.

4.4 Newton Method Results for Closed and Unbounded Mediums

It is expressed as before, Born method has some drawbacks. It requires some restrictions to be hold. Therefore, a more advanced method called Newton is practiced throughout this part.

Let us examine the Born performance on a simple case where high contrast objects are investigated. At *1 GHz*, a lossless dielectric having a permittivity of *3* and radius of *6 cm* is placed on center of PEC surrounding in Figure 4.17. Conducting radius is

45 cm. Forty observers are on a radius of *36 cm* ($\Delta_{\rho a}=0.25\lambda$). Five transmitters are located on a radius of *24 cm*. A rectangular reconstruction area in size of *24 cm* spans scatterers conceivably. Not to forget, Born results in better when contrast and/or operating frequency are low.

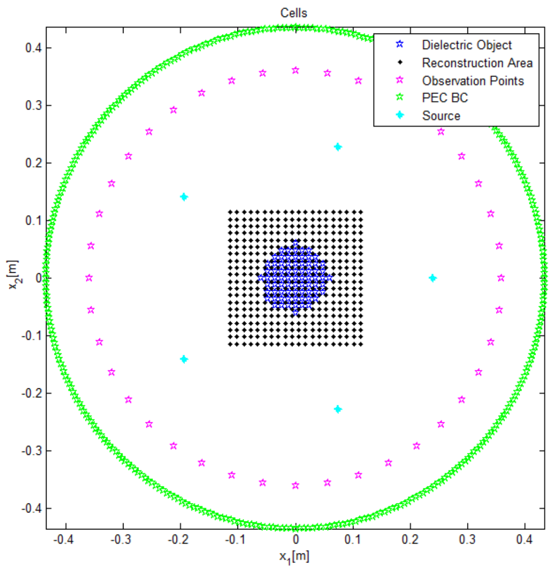

Figure 4.17 : A high contrast object is inserted into a conducting enclosure.

For closed and free space mediums, imaging is carried out using Born Approximation in Fig. 4.18. It states that Born method does not work for high contrast objects. Therefore, Newton procedure is applied using same parameters. It is important to select initial value of object function. For this example, it is assumed to be *1.5*. Tikhonov regularization is also required to be proceeded. The regularization factor *"α"* is set to 10^{-2}. The results are given in Fig. 4.19.

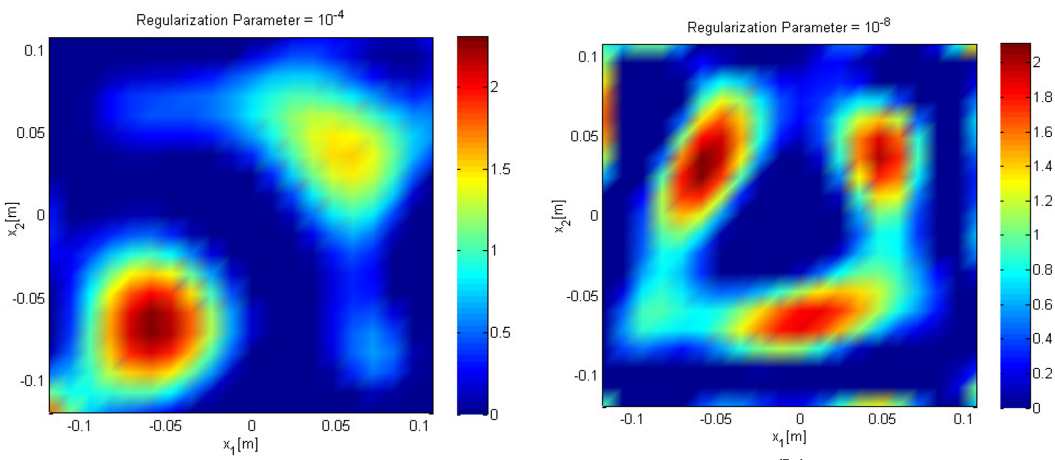

(a) **(b)**

Figure 4.18 : The real parts of object function obtained using BA for (a) closed (b) free space medium involves high contrast scatterer.

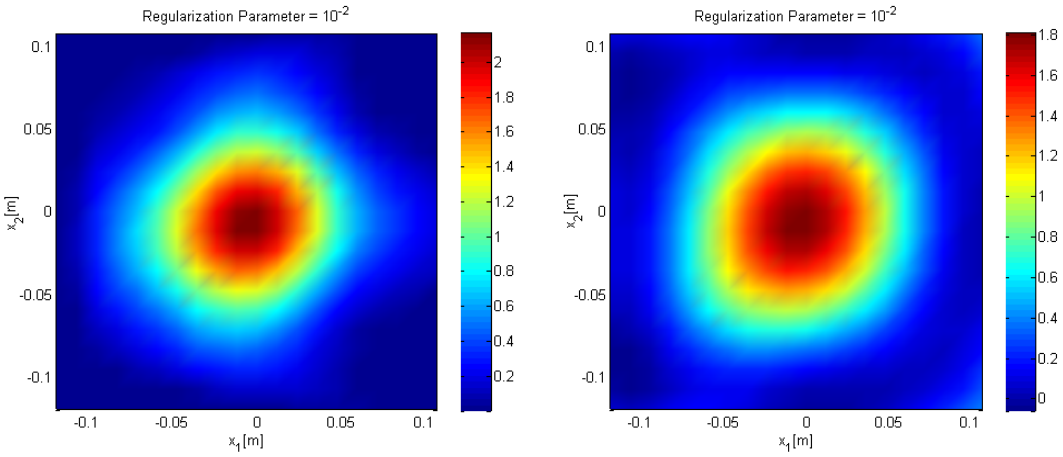

(a) **(b)**

Figure 4.19 : The real parts of object function obtained using Newton method for (a) closed (b) free space medium involves high contrast scatterer.

Ref. [13] states some examples using MR-CSI method in closed and unbounded mediums. The outcome of [13] is that these two configurations provides good reconstruction. To observe the consequences using Newton method, a square dielectric object reconstruction is exercised when background medium is filled by a dielectric material. Let us visualize the example. At *1 GHz*, a square dielectric scatterer permittivity of "$\varepsilon_{r_{obj}}=2$" is put in simulation area having a relative permittivity of "$\varepsilon_b=3$". The each side of square is around *14 cm (0.8λ)*. A PEC boundary radius of *35 cm (2λ)* surrounds the scatterer. Forty observation points are located on a circle radius of *30 cm (1.75λ)*. Five line sources are injected into simulation area at a distance of *28 cm (1.65λ)*. The scattered field data is collected on observers. Then, reconstruction area is determined as *20 cm (1.2λ)* for each side. The initial guess for object function is picked as *0.2*. When $\|\delta\upsilon\|$ is close enough to real one, iteration is stopped.

Fig. 4. 21 shows that free space solution is slighty better in geometry reconstruction, but value of contrast is worse than outcome of closed medium. The real value of object function shoulde be "$\upsilon=-0.3$".

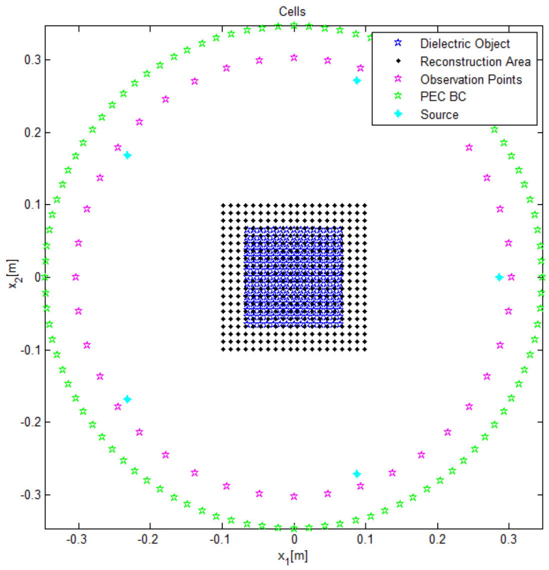

Figure 4.20 : A square dielectric object exists in a conducting enclosure.

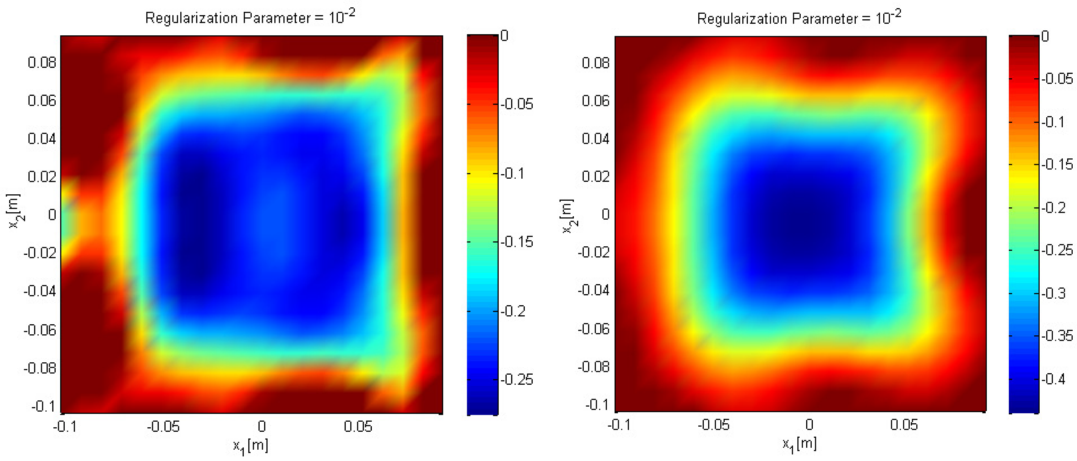

(a) **(b)**

Figure 4.21 : The real parts of object function obtained for (a) closed (b) unbounded medium relative permittivity of *"3"*.

As a last example, multi-scatterer investigation is realized. Similar setup in [13] is established. At *1 GHz*, two circular dielectric objects ($\varepsilon_{r_{obj}}=5$) in radius of *4 cm* is inserted into conducting surrounding having a radius of *30 cm*. The background is now not a free space, its relative permittivity is "$\varepsilon_b=4$". Forty observation points are in a radius of *23 cm*. In addition, ten source points are placed in a circle of radius of *25 cm*. The reconstruction area is chosen as *28 cm* for each side. Initial guess value for object function is *0.1*. It is drawn in Figure 4.22.

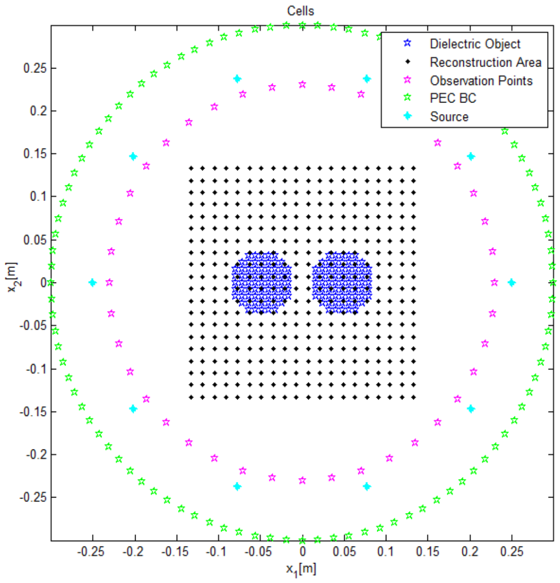

Figure 4.22 : A sample is to observe an effect of multi-scatterers using Newton method.

The value of contrast should be *0.25*. The results related to this sample is plotted in Figure 4.23.

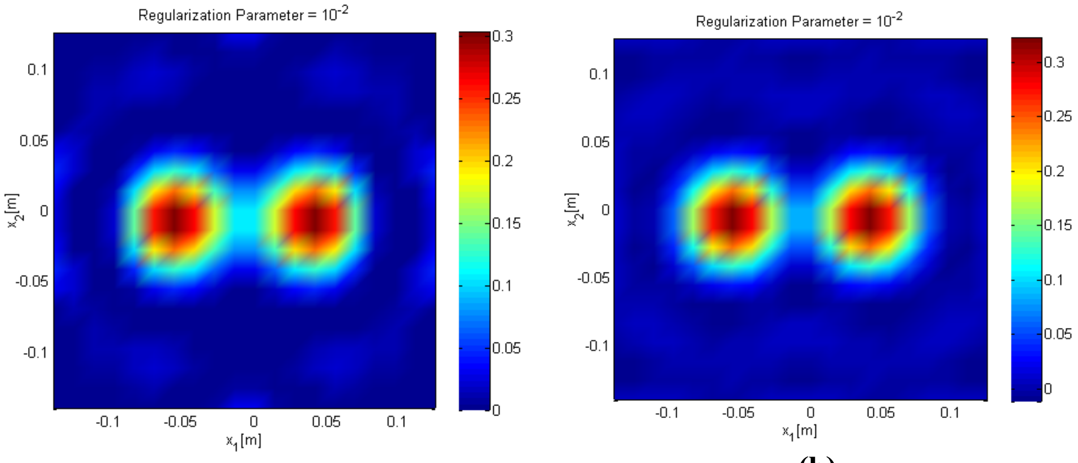

Figure 4.23 : The real parts of contrast obtained for (a) closed (b) unbounded medium having a relative permittivity of *"4"*.

Next, inside of enclosure is filled with free space and relative permittivities of scatterers are changed to "$\varepsilon_{r_{obj}}=3$". The initial guess of object function is also altered to *1.5*. Applying inversion technique, for the same $\|\delta\upsilon\|$ value closed and unbounded mediums are plotted in Fig. 4.24. The localization is found but geometry is not found for free space medium. The closed medium solution gives better reconstruction in finding geometry. So, $\|\delta\upsilon\|$ is decreased for free space. Although the reconstruction of geometry is improved, contrast of scatterer is deteriorated.

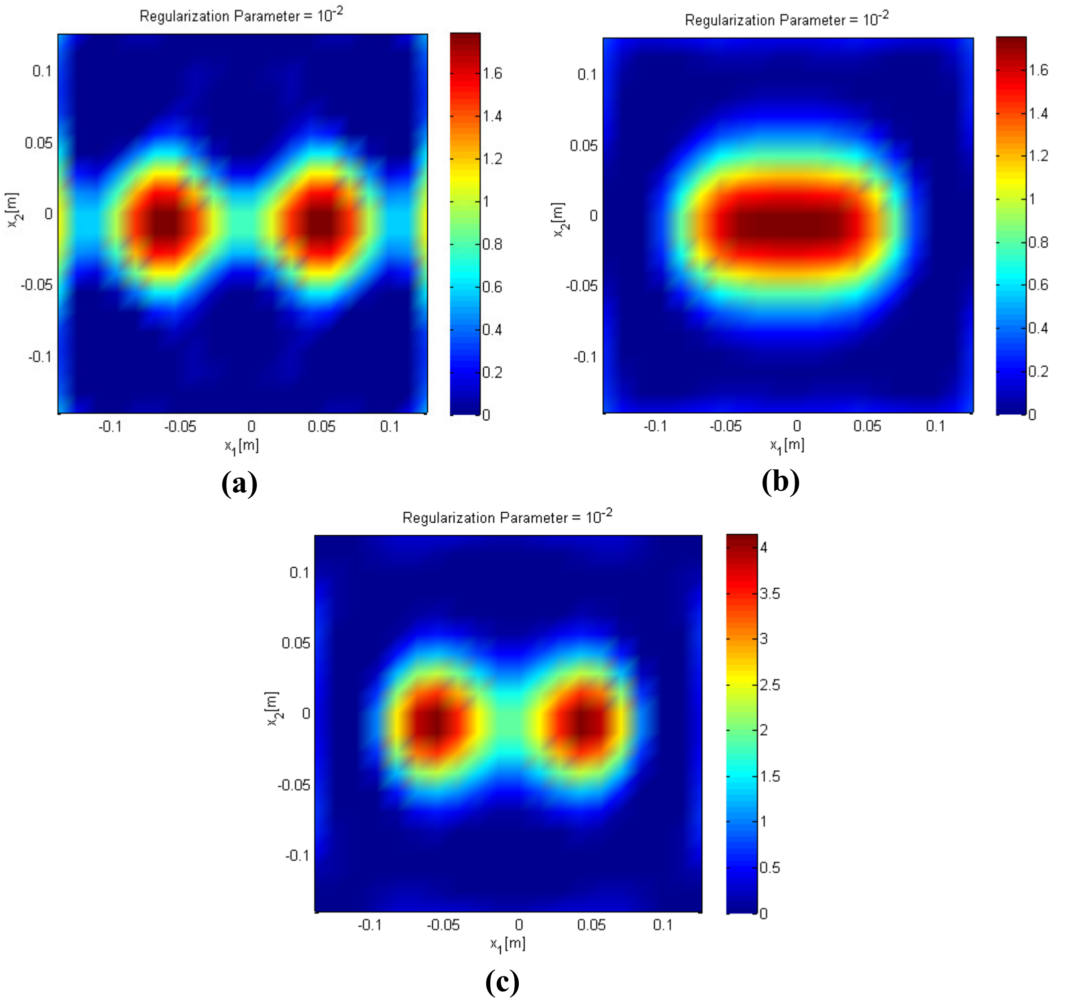

Figure 4.24 : The real parts of contrast obtained for (a) closed medium $\|\delta\upsilon\|$ *=0.80.* (b) free space $\|\delta\upsilon\|$ *=0.80*. (c) free space $\|\delta\upsilon\|$ *=0.25*.

5. CONCLUSIONS

This thesis discussed the subject of imaging of arbitrary objects located in a closed medium. In addition, reconstruction is performed for an unbounded medium eliminating conducting boundary. The outcomes are discussed and compared via various examples. For this purpose, Green's function of closed medium is found at first. Next, forward problem solution is done to acquire scattered field data thanks to Method of Moments. To validate the accuracy of MoM, analytic solution is carried out for a special case. The suitable cell size for discretization and limits of infinite series are also examined.

Besides, Born Approximation and Newton methods are utilized to find object profiles for inverse scattering problems. BA is a very simple and useful method when some restrictions are satisfied. If operating frequency and/or contrast of sought object is low, this method works well. Its application is very easy to implement. Total field in Fredholm integral equation is replaced by incident one. Then, object function can be obtained. A single line source illumination is not good enough to imaging for some cases. Therefore, more than one 2D line sources are injected to simulation and enhancement in reconstruction is observed for both closed and unbounded mediums. The main purpose of this thesis is to evaluate the impact of PEC enclosure. Thus, radius of PEC boundary is very critical. Not only radius of PEC, but also distance between PEC and observers is vital. Observers are located at a certain distance and conducting boundary is enlarged gradually. The most suitable distance is *"λ/4"* like in mentioned by references. In addition, size of reconstruction area is explored. When reconstruction area is getting closer to observers, free space solution is hugely affected and contrast of object cannot be obtained properly. It is also claimed that multi-scatterers can be imaged. The outcomes are successful in locatization for both closed and unbounded configurations. However, when geometry and physical properties are considered, these two mediums result in better imaging for different regularization parameters. The smaller values of regularization parameter bring about some defects in closed medium. As it is declared in a very beginning of this part, Born Approximation does not work to find high contrast objects. Newton is selected as an alternative method of BA for those cases.

Newton method is a more general approach that solves inverse problems iteratively. There is no approximation or restriction, so it is more complicated. MWT examples can be achieved thanks to this method. Newton procedure begins with a guessing of an initial value for object function. In every step, object function is updated and tried to get closer to its real value. Both closed and unbounded mediums provide similar results in localization. Then two close scatterers are investigated. For high contrast objects, error tolerance of object function is set to a specified value. Then, unbounded medium cannot resolve geometry of object. After error tolerance is decreased for unbounded case, geometry is obtained. However, contrast of sought objects is not achieved correctly. Closed medium provides better enhancement in reconstruction for those cases.

All in all, low contrast object imaging is not well improved when medium is surrounded by a conducting. However, better reconstruction of high contrast objects is performed by means of a conducting enclosure. For the further study, solution of 3D inverse scattering problem in closed medium can be implemented using different inversion algorithms.

REFERENCES

[1] **Chew, W. C., and Wang, y. M.** (1990). Reconstruction of Two-Dimensional Permittivity Distribution Using the Distorted Born Iterative Method. *IEEE Transactions On Medical Imaging*, Vol. ***9***, No. 2.

[2] **Kleinman, R. E., and Wang, y. P. M.** (1997). A Contrast Source Inversion Method. *Inverse Problems*, Vol. ***13***, pp. 1607-1620.

[3] **Abubakar, A., van den Berg, Pe. M., Mallorqui, J. J.** (2002). Imaging of Biomedical Data Using a Multiplicative Regularized Contrast Source Inversion Method. *IEEE Transactions On Microwave Theory And Techniques*, Vol. ***50***, No. 7.

[4] **Yapar, A.**, (2006). A regularized Newton method for one-dimensional profile inversion of a lossy cylinder. *AEU-International Journal of Electronics and Communications*, Vol. ***60***, pp. 590-595.

[5] **Soldovieri, F., and Solimene, R.** (2007). Through-Wall Imaging via a Linear Inverse Scattering Algorithm. *IEEE Geoscience And Remote Sensing Letters*, Vol. ***4***, no. 4.

[6] **Ament, W. S.** (1956). Forward- and Back-Scattering From Certain Rough Surfaces. *IEEE Transactions on Antennas and Propagation*, Vol. ***4***, no. 3, pp. 369–373, July 1956. 7.

[7] **Hadamard, J.** (1902). On problems for Partial derivatives and their physical meaning. *Princeton University Bulletin*, pp. 49-52, 1902.

[8] **Klema, V. K., and Laub, A. J.** (1980). The Singular Value Decomposition: Its Computation and Some Applications. *IEEE Transactions On Automatic Control*, Vol. **25**, no. 2, pp. 164-176.

[9] **Engl, H. W., Hanke, M., and Neubauer, A.** (1996). *Regularization of Inverse Problems*, Springer.

[10] **Tikhonov, A. N., and Arsenin, V. Y.** (1977). *Solutions of Ill-Posed Problems. Winston*, Washington, D. C.

[11] **Kress, R., Yaman, F., Yapar, A., and Akduman, I.** (2009). Inverse scattering for an impedance cylinder buried in a dielectric cylinder. *Inverse Problems In Science And Engineering*, Vol. ***17***, no. 4, pp. 473-488.

[12] **Cakoni, F., and Monk, P.** (2006). The 3D Inverse Electromagnetic Scattering Problem for a Coated Dielectric. *Numerical Mathematics and Advanced Applications*, Springer Link, pp. 119-134.

[13] **Gilmore, C., and LoVetri, J.** (2008). Enhancement of microwave tomography through the use of electrically conducting enclosures. *IOPscience, Inverse Problems*, Vol. ***24***, no. 3.

[14] **Mojabi, P., and LoVetri, J.** (2011). A Novel Microwave Tomography System Using a Rotatable Conductive Enclosure. *IEEE Transactions On Antennas And Propagation*, Vol. ***59***, no. 5.

[15] **Larsen, L. E., and Jacobi, L. H.** (1986). Medical Applications of Microwave Imaging. *New York: IEEE Press*, May.

[16] **Richmond, J. H.** (1965). Scattering by a dielectric cylinder of arbitrary cross section shape. *IEEE Transactions on Antennas and Propagation*, Vol. ***13***, Issue. 3.

[17] **Crocco, L., and Litman, A.** (2009). On embedded microwave imaging systems: retrievable information and design guidelines. *IOPscience, Inverse Problems*, Vol. ***25***, no. 6.

[18] **Takada, J.** (n.d.). Wave Theory II — Numerical Simulation of Waves — (2) Representation of Wave Function by Using Green Function — (I) Green's Theorem and Free Space Green Function. Date retrieved: 25.06.2014,
address: http://www.ap.ide.titech.ac.jp/~takada/waves/text2.pdf

[19] **Balanis, A. C.** (1989). Advanced Engineering Electromagnetics. *John Wiley & Sons*.

[20] **Caorsi, S., Costa, A., and Pastorino, M.** (2001). Microwave Imaging Within the Second-Order Born Approximation: Stochastic Optimization by a Genetic Algorithm. *IEEE Transactions On Antennas And Propagation*, Vol. 49, No. 1.

CURRICULUM VITAE

Name Surname: Gizem DİLMAÇ

Place and Date of Birth: Mersin / 04.01.1990

Address: Acıbadem - ÜSKÜDAR

E-Mail: dilmacgizem@gmail.com

B.Sc.: Electronics and Communications Engineering

Computer Engineering / Doğuş University

PROFESSIONAL EXPERIENCE AND REWARDS:

Doğuş University – Research Assistant (March 2013 – Sept. 2014)

Huawei Technologies – Software Engineer (Nov. 2013 – March 2013)

~

Doğuş University - The Faculty of Engineering First Place Honor Degree (July 2012)

PUBLICATIONS/PRESENTATIONS ON THE THESIS

- Dilmac G., Yapar A., 2014: Kapalı Ortamlara Gömülü Cisimlere İlişkin Elektromanyetik Ters Saçılma Problemleri. *VII URSI-Türkiye Bilimsel Kongresi*, August 28-30, 2014 Elazığ, Turkey.